Effect of turbulence on the drag and lift of a particle

P. Bagchi and S. Balachandar

Department of Theoretical and Applied Mechanics

University of Illinois at Urbana-Champaign,

Urbana, IL 61801, USA

Key words: Multiphase flows, turbulence, particulate flows, drag and lift, particle–turbulence interaction

Abstract

A direct numerical simulation (DNS) is used to study the effect of a freestream isotropic turbulent flow on the drag and lift forces on a spherical particle. The particle diameter is about 1.5 to 10 times the Kolmogorov scale, the particle Reynolds number is about 60 to 600, and the freestream turbulence intensity is about 10 to 25%. It is shown that the freestream turbulence does not have a substantial and systematic effect on the time-averaged mean drag. The standard drag correlation based on the instantaneous or mean slip velocity results in a reasonably accurate prediction of the mean drag obtained from the DNS. However, the accuracy of pre-

diction of the instantaneous drag decreases with increasing particle size. For the smaller particles, the low frequency oscillations in the DNS drag are well captured by the standard drag, but for the larger particles significant differences exist even for the low frequency components. Inclusion of the added-mass and history forces, computed based on the fluid velocity at the center of the particle, does not improve the prediction. Different estimates of the fluid velocity seen by the particle are examined. It is shown that the mean drag is insensitive to the fluid velocity measured at the particle center, or obtained by averaging over a fluid volume of the order of the particle size. The fluctuations diminish as the size of the averaging volume increases. The effect of increasing freestream turbulence intensity for the same particle size is studied. Fluctuations in the drag and lift forces are shown to scale with the mean drag and freestream intensity. The standard drag without the added-mass and history forces provides the best approximation to the DNS result.

I. Introduction

Dispersed particulate flows abound in nature and in engineering applications. In most cases, the fluid phase is turbulent. The interaction between the fluid phase and the particulate phase is bi-directional: the carrier-phase turbulence influences the dispersion and preferential accumulation of the particles which in turn modulate the fluid turbulence. At the level of a single particle, the effect of freestream turbulence is to modify the drag force compared to that in a steady uniform flow (often called "standard drag"). On the other hand, a particle can modify freestream turbulence by the formation of a wake, periodic shedding of vortices, and wake turbulence. The collective effect of the presence of a distribution of particles can further modify the effective drag force on a particle due to screening effect and thereby influence the mean settling and dispersion characteristics. Similarly, the collective effect of the dispersion of particles will determine the attenuation or augmentation of the fluid turbulence.

In this paper we will address the effect of the freestream turbulence on the drag and lift forces on a single particle. We choose to investigate the simplest case of an isotropic freestream turbulence of Taylor microscale Reynolds number equal to 164. The two important parameters of the problem are then the ratio of the particle diameter d to the Kolmogorov scale η, and the intensity of freestream turbulence defined as the ratio of the root-mean-square (rms) turbulent fluctuation to the mean relative velocity between the particle and the surrounding fluid. The diameter of the particle under consideration is varied from about 1 to 10 times the Kolmogorov

scale, and the turbulence intensity is varied from 10 to 25%. Consequently the particle Reynolds number, based on the relative velocity and particle diameter, is in the range 60 to 600.

Consider the case of a particle settling through a turbulent flow. The mean settling velocity of the particle provides a convenient measure of the mean drag force. In experiments the mean drag coefficient is computed based on the measurement of the mean settling velocity V_T and a force balance between the gravity and the drag force as:

$$C_D = \frac{4}{3} g d (\rho - 1) \frac{1}{V_T^2}, \tag{1}$$

where ρ is the particle-to-fluid density ratio, and g is the acceleration due to gravity. If the ambient flow is stagnant, V_T corresponds to the terminal velocity and the above relation yields the standard drag coefficient corresponding to a uniform nonturbulent flow. In a turbulent flow, however, there are two well understood mechanisms that influence the mean settling rate. The first is due to the non-linear dependence of the drag on the relative velocity at finite Reynolds numbers. For the same density ratio ρ and diameter d, the mean settling velocity in a turbulent flow is less than that in a stagnant flow (Mei, Adrian & Hanratty[1]). The settling velocity decreases with increasing turbulence intensity and the resulting mean drag as given by (1) is higher than that based on the terminal velocity in a stagnant flow. This effect will decrease with decreasing Reynolds number and will entirely vanish in the linear Stokes limit. The second, and more complex, mechanism is due to the preferential trajectories of freely falling particles. Particles do not sample the turbulent flow uniformly, but

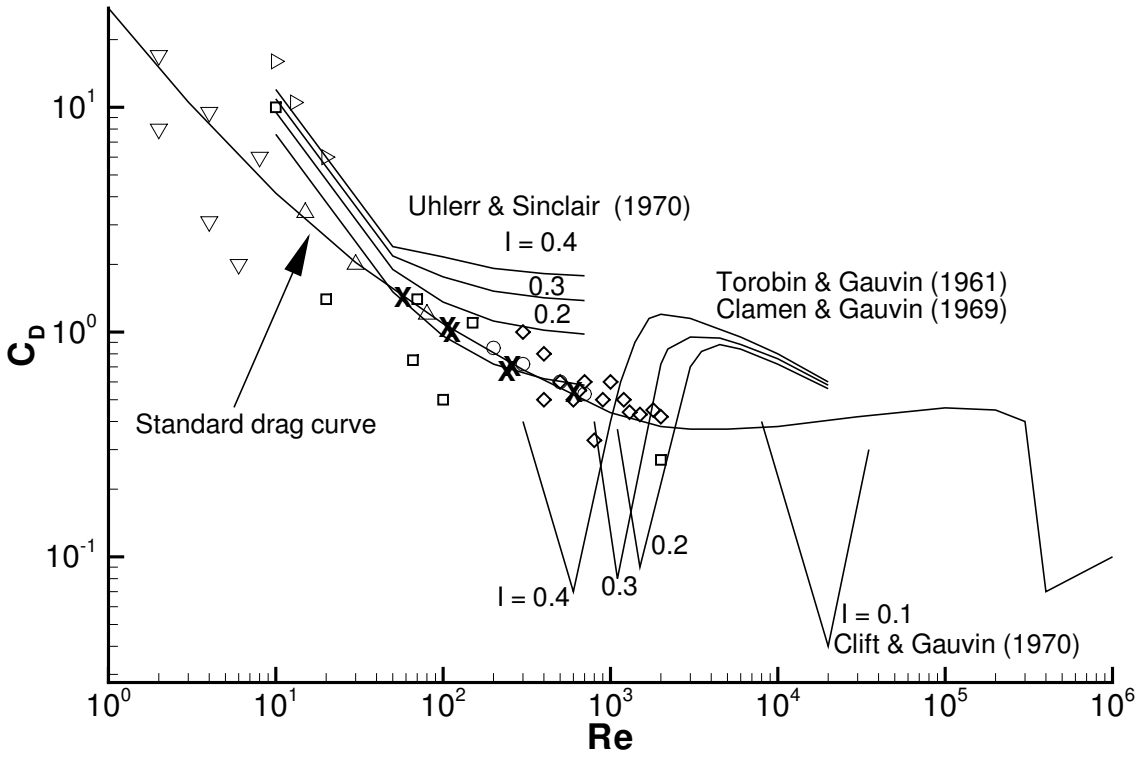

Figure 1: A summary of the results on the effect of turbulence on the drag coefficient. $\times$ Present results; $\square$ Gore & Crowe;[15] $\diamond$ Sankagiri & Ruff;[16] $\circ$ Zarin & Nichols;[4] Δ Warnica *et al.*;[8] ∇ Rudolf & Bachalo;[7] $\triangleright$ Brucato *et al.*.[5]

prefer regions of downwash compared to regions of up-moving fluid (see Wang & Maxey[2]). Thus the mean fluid velocity seen by a particle differs from the true mean obtained by averaging over the entire volume of fluid. Unlike the effect of nonlinear drag dependence, the effect of preferential trajectory is to increase the mean settling velocity. Thus the drag coefficient evaluated based on (1) tends to be lower due to the effect of preferential trajectory.

The effect of nonlinear drag dependence is important for particles larger than

the Kolmogorov scale (Mei, Adrian & Hanratty[1]), while the preferential bias is dominant for small particles of size comparable to or smaller than the Kolmogorov scale (Wang & Maxey[2]). These two competing mechanisms can at least partially explain the large scatter of experimental data on the drag coefficient in turbulent flows shown in figure 1. Also plotted in the same figure for reference is the standard drag correlation applicable for the case of a stationary or steadily moving particle in a steady uniform ambient flow. The scatter in the data clearly illustrates the degree of disagreement as to the effect of turbulence. For example, in the moderate Reynolds number regime, the measurements of Uhlher & Sinclair,[3] Zarin & Nichols,[4] and Brucato *et al.*[5] observed a substantial increase in the drag coefficient in a turbulent flow. The numerical study by Yusof[6] also observed a drag increase of nearly 40% by the freestream turbulence of 20% intensity. On the other hand, the results of Rudolff & Bachalo[7] tend to suggest a reduction in the drag coefficient due to ambient turbulence. In contrast, Warnika *et al.*[8] suggest that the drag on a spherical liquid drop is not significantly different from the standard drag. The experiments of Wu & Faeth[9,10] also suggest little influence of turbulence on the mean drag. The experiments of Torobin & Gauvin,[12] Clamen & Gauvin,[13] Clift & Gauvin[14] pertain to particle Reynolds numbers greater than 1000 which is beyond the range of particulate flows. In this range they observed an early transition to turbulence in the boundary layer of a particle resulting in a sudden drop in the drag coefficient.

It should be noted that the effects of nonlinear drag dependence and trajectory bias can be easily accounted for, provided the drag coefficient is evaluated on

an instantaneous basis using (1), with the instantaneous slip velocity between the particle and the surrounding fluid replacing the mean settling velocity V_T. The instantaneous drag coefficient thus evaluated may still differ from the standard drag, due to the effect of convective and temporal accelerations of the fluid and the particle, which give rise to the added-mass and the history forces. More importantly, the complex interaction between the various scales of turbulent flow with the particle can strongly influence the instantaneous drag. In the experimental results discussed above this inherent effect of turbulence is also present apart from the effects of non-linear drag dependence and trajectory bias. In this paper we plan to focus on this inherent influence of turbulence in modifying the mean and instantaneous drag.

We consider the effect of turbulence on the forces on a stationary particle subjected to an isotropic turbulent flow which along with a uniform flow is applied as the freestream flow. The problem set-up is very similar to the one considered in the experiments of Wu & Faeth,[9,10] where a stationary particle was subjected to homogeneous turbulence. The range of parameters chosen in our study, which are mentioned previously, also matches with those of Wu & Faeth.[9,10] The present set-up and parametric range are also similar to the ones considered by Mittal,[17] who performed numerical simulation of a stationary particle subjected to an oscillating uniform flow in lieu of a turbulent freestream.

The present methodology allows one to isolate the different mechanisms of drag modification by turbulence. First, by considering a stationary particle the effect of the trajectory bias is avoided. Second, the freestream turbulent flow to which the

particle is subjected is computed from a separate simulation and hence is known *a priori*. As a result the time history of the relative velocity between the particle and the ambient flow is known, and hence, the effect of nonlinear drag dependence can be precisely accounted for. The effect of the added-mass and history forces can also be accounted for from the precomputed turbulent field. The accuracy of the standard drag correlation in predicting the DNS drag can then be evaluated. Any discrepancy away from the standard drag correlation can be interpreted as the inherent influence of turbulence.

In this paper, we present the DNS results on the mean and instantaneous drag and compare them with the predictions based on the standard drag correlations such as the Schiller–Neumann formula (see Clift *et al.*[18]):

$$C_D = \frac{24}{Re}(1 + 0.15Re^{0.687}) \,. \tag{2}$$

We consider the effect of varying the particle size and turbulence intensity, and as a result, the particle Reynolds number. The effect of including the added-mass and history forces with the Schiller-Neumann drag is also studied. The effect of different approximations for the fluid velocity seen by the particle is examined. The rms, mean squared difference, and cross-correlation of the DNS results and various predictions are presented. The DNS technique employed here is described in the following section. The results on the instantaneous drag, and the corresponding mean are given in section III. Summary and conclusion are presented in section IV.

II. Methodology

We consider interaction of a *single* spherical particle with isotropic turbulence. The turbulent field is a precomputed 256^3 DNS data in a $(2\pi)^3$ box obtained by Langford.[19] The field is periodic along all three directions and hence can be extended to any arbitrary large volume. The parameters that characterize this isotropic turbulence are as follows: root mean square of the turbulent velocity fluctuation is 5.2345, the Kolmogorov scale $\eta = 0.0083$, dissipation $\epsilon = 62.9$, Taylor microscale $\lambda = 0.209$, and the microscale Reynolds number $Re_\lambda = 164$.

An instantaneous realization of the isotropic field is considered and is represented by $\mathbf{U}(\mathbf{X})$, where (X, Y, Z) is a fixed reference frame attached to the isotropic turbulent field. The turbulent field is superposed on a steady uniform freestream $\mathbf{V}$. Without loss of generality we assume that $\mathbf{V}$ is oriented along the X-axis. In a reference frame (x, y, z) whose origin is fixed on to the center of a stationary particle the undisturbed ambient flow appears as $\mathbf{V} + \mathbf{U}(\mathbf{x} + \mathbf{X}_p(t))$, where $\mathbf{X}_p(t) = \mathbf{X}_p(0) - \mathbf{V}t$ is the instantaneous location of the center of the particle in the frame attached to the isotropic turbulent field. In other words, the turbulent field $\mathbf{U}(\mathbf{X})$ is swept past the stationary particle at the velocity $\mathbf{V}$. The computational domain attached to the particle is a spherical domain (r, θ, ϕ) whose outer radius R_O is 30 times the radius of the particle. The undisturbed ambient flow, as defined above, is specified at the inflow section of this outer boundary. A schematic view of the computation domain attached to the particle and the precomputed turbulent field is shown to scale in figure 2 for the case of $d/\eta = 10$. In general, the grid points of the spherical

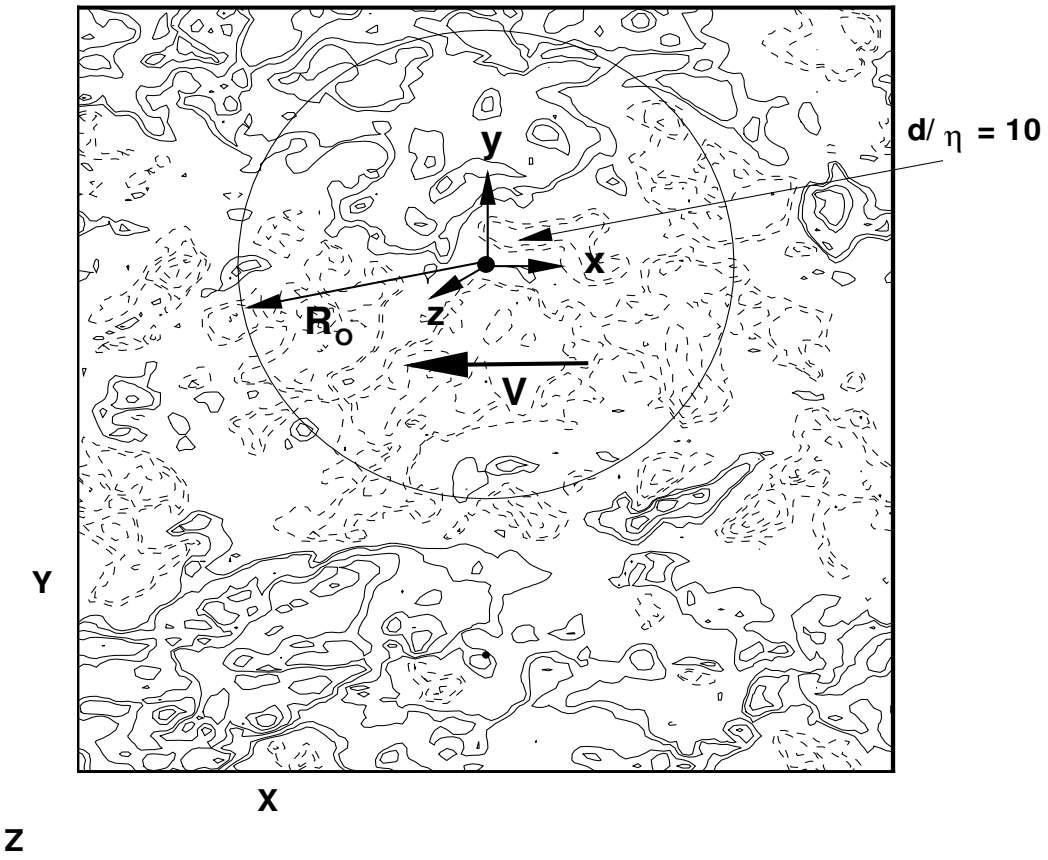

Figure 2: Schematic of the particle-flow configuration. Drawn to the true scale, a particle of $d/\eta = 10$ is shown here. The large circle surrounding the particle represents the outer boundary of the spherical computational domain attached to the particle. The outer box represents the $(2\pi)^3$ box in which the isotropic turbulent flow is generated. Contours of one cross-stream velocity component scaled by $\langle|\mathbf{V}_r|\rangle$ are show for $I = 0.1$.

computational domain attached to the particle do not coincide with the grid points of the $(2\pi)^3$ cubic box in which the isotropic turbulent field is computed. Thus the turbulent velocity field $\mathbf{U}(\mathbf{X})$ has to be interpolated on to the outer boundary of the spherical domain. In order to retain spectral accuracy, the interpolation is done using Fourier summation.

It must be stressed that here we use an instantaneous three-dimensional field of precomputed isotropic turbulence to supply the turbulent inflow condition for the particle. Instead, an inflow could have been constructed as a uniform flow with superposition of a spectrum of modes with time varying amplitudes to mimic the desired turbulence properties. Although somewhat computationally complicated, the application of the precomputed frozen isotropic box turbulence as the inflow condition provides a well defined turbulent ambient flow which is characterized by a single parameter, the microscale Reynolds number.

In the spherical domain attached to the particle, the governing (continuity and Navier-Stokes) equations are solved by a direct numerical simulation. A Fourier-Chebyshev collocation scheme in the spherical coordinates is used for the spatial discretization, and a two-step time-split scheme is used for the temporal discretization. Further details about the collocation method are given in Bagchi & Balachandar.[20] At the outflow boundary of the spherical domain, a non-reflecting boundary condition described by Mittal & Balachandar[21] is used. On the surface of the particle no-slip and no-penetration conditions are satisfied. The distribution of the grid points is non-uniform: they are clustered near the surface of the particle and in the

wake region. The grid resolution is chosen to satisfy two criteria: first, the size of the largest grid in the spherical domain is less than that of the grid used to simulate the isotropic turbulent field, in order to guarantee resolution of the freestream turbulence. Second, the grid is adequate to resolve the thin shear layers and the wake structures generated by the particle. Typical grids used in the simulation have 141 points in the radial direction, 160 in the θ-direction and 128 in the ϕ direction.

In order to get well converged statistics, the entire 2π length of the cubic box of turbulence is passed over the particle several times. This ensures that any initial transience from the start-up decays, and that a long time periodic behavior is established. The length of the turbulence box can vary from about 150 to 1000 times the diameter of the particle. A typical dimensionless time-step $\Delta t|\mathbf{V}|/d$ used in the simulations is 0.0005. Thus the total number of time-steps for which time integration is performed is of the order of 10^6. This combined with the high grid resolution renders the computations very expensive. A typical computation time for a simulation is about 20,000 CPU hours on Origin2000 supercomputers using 32 processors.

The time-averaged mean quantities are obtained by averaging over a time T that the periodic box of turbulence takes to pass over the particle. The mean quantities are denoted by the symbol $\langle\rangle$. The parameters of this problem are the ratio of the particle diameter to the Kolmogorov scale of the isotropic turbulence d/η, the turbulence intensity defined as $\tilde{I} = U_{rms}/|\langle\mathbf{V}_r\rangle|$, and the mean particle Reynolds number $\langle Re_r\rangle = |\langle\mathbf{V}_r\rangle|d/\nu$, where U_{rms} is the rms of the fluctuations of

the freestream turbulence, $\mathbf{V}_r = \mathbf{V} + \mathbf{U}(\mathbf{X}_p(t))$ is the instantaneous relative (slip) velocity between the particle and the undisturbed ambient flow measured at the center of the particle, and $\langle \mathbf{V}_r \rangle$ is the mean slip velocity obtained by time-averaging over T. Note that although the isotropic turbulent velocity averaged over the entire box is guaranteed to be zero, the mean turbulent velocity seen by the particle, $\langle \mathbf{U}(\mathbf{X}_p(t)) \rangle$, may be non-zero due to the limited volume sampled by the particle. The mean particle Reynolds number can be expressed in terms of the other two parameters as

$$\langle Re_r \rangle = \frac{d/\eta}{\tilde{I}} \frac{U_{rms}}{v_k}, \tag{3}$$

where v_k is the Kolmogorov velocity scale. For the isotropic turbulent flow considered here the velocity ratio $U_{rms}/v_k = 6.5$. Here we discuss the results of six different simulations covering a range of parameter values given in table I. The diameter of the particle is varied from about 1.5 to 10 times the Kolmogorov scale. Thus in all the cases considered the particle is bigger than the Kolmogorov scale but smaller than the Taylor micro-scale. The turbulence intensity is varied from 9 to 26%, and the resulting mean Reynolds number varies from about 60 to 610. We also define a modified freestream intensity as $I = U_{rms}/|\mathbf{V}|$ which is also given in the table. The parametric range chosen for the present study is in reasonable agreement with many previous works that are aimed at studying particle-turbulence interaction (see table II). A variety of flows ranging from homogeneous turbulence to pipe flow, channel flow, and jets have been studied. In many of these studies the particle size ranges from about the Kolmogorov scale up to the Taylor microscale (Tsuji *et al.*,[22] Wu &

Case	d/η	d/λ	d/Λ	$\tilde{I} = U_{rms}/\langle\|\mathbf{V}_r\|\rangle$	$I = U_{rms}/\|\mathbf{V}\|$	$\langle Re_r \rangle$
Case 1	1.53	0.061	0.003	0.093	0.1	107
Case 2	1.53	0.061	0.003	0.171	0.2	58
Case 3	3.84	0.152	0.008	0.096	0.1	261
Case 4	3.84	0.152	0.008	0.219	0.25	114
Case 5	9.59	0.381	0.019	0.103	0.1	609
Case 6	9.59	0.381	0.019	0.259	0.25	241

Table I: Parametric range of the present study. η= Kolmogorov scale; λ = Taylor microscale; Λ = integral scale.

Faeth,[9,10] Mizukami *et al.*,[23] Parthasarathy & Faeth,[24] Yusof[6]). In many of these studies the focus has been the interaction of turbulence with a distribution of large number of particles. Of particular relevance to the present study is the experimental work of Wu & Faeth[9,10] who considered the interaction of a single particle subjected to homogeneous turbulence.

III. Effect of turbulence on drag

A. Mean drag

The instantaneous force on the particle is computed in the DNS by integrating the pressure and shear stresses on the surface of the particle as:

$$\mathbf{F}(t) = \int_S \left[-p\,\mathbf{e}_r + \tau_{r\theta}\,\mathbf{e}_\theta + \tau_{r\phi}\,\mathbf{e}_\phi\right]\,\mathrm{d}S\,, \tag{4}$$

The component of this force along the direction of the instantaneous relative velocity $\mathbf{V}_r$ is the instantaneous drag force, F_D, and the normal component is the instantaneous lift force, F_L. Note that the instantaneous relative velocity and hence the drag force constantly changes direction, although they are oriented nearly along

Experiments	d/η	d/λ	I	$\langle Re_r \rangle$
pipe flow *	2–60	0.13–2	0.05–0.15	
homogeneous turbulence **	1.2–12	0.13–2	0.04–0.07	135–1560
homogeneous turbulence †	1.2–8		0.02–0.08	38–545
particle-laden jet ††			0.05–0.15	100–750
particle-laden jet ‡	7–29 +			
channel flow ‡‡	0.57–3 +		0.05–0.2	5–20
Stirred vessel ++	1.5–35			0.2–40
isotropic (frozen) ◇	5.2–14.3		0.03–0.19	100

Table II: Some experimental works on particle-flow interaction and their parametric range. Here + indicates that the number is τ_p/τ_f, the ratio of particle response time to fluid time-scale. * Tsuji *et al.*;[22] ** Wu & Faeth;[9,10] † Parthasarathy & Faeth;[24] †† Tsuji *et al.*;[31] ‡ Longmire & Eaton;[28] ‡‡ Kulick *et al.*;[27] ++ Brucato *et al.*;[5] ◇ Yusof.[6] Note that Yusof's[6] work is a numerical investigation.

the x-axis since $U_{rms}/|\mathbf{V}|$ considered here is at the most 25%. The mean drag force from the DNS data is evaluated as

$$\langle F_D \rangle = \langle |\mathbf{F}(t) \cdot \widehat{\mathbf{V}}_r| \rangle \,, \tag{5}$$

where $\widehat{\mathbf{V}}_r$ is the unit vector along the relative velocity. The dimensionless mean drag coefficient is computed by

$$C_D = \frac{\langle F_D \rangle}{\frac{1}{2}\rho\pi a^2 \langle |\mathbf{V}_r| \rangle^2}, \tag{6}$$

The DNS result on the mean drag coefficient is presented in figure 1, along with the past experimental results. The present DNS results compare reasonably well with the standard drag curve implying that the freestream turbulence does not have a substantial effect on the mean drag at least over the range of Reynolds number considered.

A more quantitative comparison is presented in Table III, where the DNS result is compared with two different estimates based on the standard drag correlation by Schiller & Neumann (Clift *et al.*[18]) as given in (2). The first estimate is obtained by applying the Schiller-Neumann formula to compute the instantaneous drag from the time-dependent relative velocity $\mathbf{V}_r$ and Reynolds number $Re_r(t) = |\mathbf{V}_r|d/\nu$, and then averaging over time T. The second estimate is based on the time-averaged relative velocity $\langle \mathbf{V}_r \rangle$ and Reynolds number $\langle Re_r(t) \rangle$ applied directly to the Schiller-Neumann formula (2). These estimates can be expressed as

$$\text{Estimate 1} \quad : \qquad \langle F_D \rangle_1 = \langle \frac{1}{2} \rho \pi a^2 \, C_D(Re_r) \, |\mathbf{V}_r|^2 \rangle \, , \tag{7}$$

$$\text{Estimate 2} \quad : \qquad \langle F_D \rangle_2 = \frac{1}{2} \rho \pi a^2 \, C_D(\langle Re_r \rangle) \, |\langle \mathbf{V}_r \rangle|^2 \, , \tag{8}$$

where

$$C_D(Re_r) \;=\; \frac{24}{Re_r} \left[1 + 0.15 Re_r^{0.687} \right] \, , \tag{9}$$

$$C_D(\langle Re_r \rangle) \;=\; \frac{24}{\langle Re_r \rangle} \left[1 + 0.15 \langle Re_r \rangle^{0.687} \right] \, . \tag{10}$$

The difference between the above two estimates highlights the effect of nonlinear drag dependence. It can be seen from Table III that both of these estimates differ from the DNS result by atmost 17%, but for most cases the difference is less than 8%. The difference does not appear to have any systematic dependence on the Reynolds number or turbulence intensity. In some cases the difference is positive and in others it is negative.

The estimate 1 differs from 2 by less than 6%, which implies that the effect of nonlinear drag dependence is minimal in the parametric range of the present

simulations. The fractional difference between the two estimates can be expressed as

$$\frac{|\langle F_D \rangle|_1 - |\langle F_D \rangle|_2}{|\langle F_D \rangle|_2} \approx \frac{0.58\alpha\langle \epsilon^2 \rangle}{1+\alpha}, \tag{11}$$

where $\alpha = 0.15\langle Re_r \rangle^{0.687}$, and the small parameter $\epsilon = \left(|\mathbf{V}_r| - |\langle \mathbf{V}_r \rangle|\right)/|\langle \mathbf{V}_r \rangle|$ measures the level of fluctuation in the freestream turbulence. By definition, $\langle \epsilon \rangle = 0$, and $I^2 = U_{rms}^2/|\mathbf{V}|^2$ provides a reasonable measure of $\langle \epsilon^2 \rangle$. The effect of nonlinear drag dependence is thus likely to be significant only at large Reynolds numbers, when α is large, and when the level of freestream fluctuation is quite strong. Based on the above equation the effect of nonlinearity for the different cases considered here can be estimated to be weak, only ranging from about 0.4% to 3.3%.

It is thus clear that freestream turbulence, at least over the range of parameters considered, has no systematic effect on the time-averaged mean drag force. Therefore, the use of the standard drag correlation, based on the instantaneous or mean slip velocity, will result in reasonably accurate prediction of the mean drag force. However, as will be discussed next, the accuracy of prediction of the instantaneous drag force will depend on both the size of the particle and the turbulence intensity.

The mean drag is however dependent on the definition of the mean fluid velocity seen by the particle. The mean fluid velocity obtained by averaging over the entire volume of fluid can result in a significantly different estimate of the mean drag if the particle does not sample the entire volume. For example, in the present simulations, the mean velocity of the entire cubic box of turbulence swept past the particle is $\mathbf{V}$.

d/η	$I = U_{rms}/\|\mathbf{V}\|$	DNS drag	Estimate 1	Estimate 2	Estimate 3
1.5	0.1	1.067	1.077	1.058	0.963
1.5	0.2	1.533	1.515	1.426	1.201
3.8	0.1	0.705	0.732	0.723	0.682
3.8	0.25	1.026	1.104	1.035	0.894
9.6	0.1	0.544	0.529	0.524	0.550
9.6	0.25	0.683	0.799	0.751	0.837

Table III: Mean drag

Similar to (7) and (8), an estimate of the mean drag based on $\mathbf{V}$ can be obtained as

$$\text{Estimate 3} \quad : \qquad \langle F_D \rangle_3 = \frac{1}{2}\rho\pi a^2 C_D(Re_p)\,|\mathbf{V}|^2 \qquad \text{where} \qquad Re_p = \frac{|\mathbf{V}|d}{\nu}\,, \tag{12}$$

which is also presented in table III. A discrepancy as high as 22% for case 2 ($d/\eta = 1.5,\ I = 0.2, \langle Re_r \rangle = 107$) is observed with respect to the DNS drag. The difference between this estimate and the one given in (8) is due to the difference in the definition of the mean fluid velocity seen by the particle. If we take the difference to be represented by a small parameter $\delta = (\mathbf{V} - |\langle \mathbf{V}_r \rangle|)\,/|\langle \mathbf{V}_r \rangle|$, then the fractional difference between the two estimates can be expressed as

$$\frac{|\langle F_D \rangle|_3 - |\langle F_D \rangle|_2}{|\langle F_D \rangle|_2} \approx \frac{\delta(1 + 1.687\alpha)}{1 + \alpha}\,. \tag{13}$$

Any uncertainty in the mean fluid velocity seen by the particle will influence the mean drag estimation linearly, and the relative turbulence intensity, I, provides a measure for the possible uncertainty in the mean fluid velocity. Thus, unlike the effect of nonlinear drag dependence where the influence of perturbation is quadratic, here it is linear. Also note that for the same level of uncertainty, the error will be 68.7% larger at higher Reynolds number than in the Stokes limit. Although

the present simulations consider only a stationary particle, the above results suggest the potential importance of preferential particle trajectory on the mean drag, if the particle was allowed to fall freely through isotropic turbulence, as in some experiments.

B. Instantaneous drag

The time history of the forces on the particle is shown in figures 3 and 4. Three different cases with the particle diameter $d/\eta = 1.5$, 3.8 and 9.6 are considered, while the turbulence intensity measured as $I = U_{rms}/|\mathbf{V}|$ is fixed at 0.1. Since the instantaneous relative velocity and hence the drag force constantly change direction it is convenient to write the net force in nondimensional form as $\mathbf{C_F} = C_x\mathbf{e}_x + C_y\mathbf{e}_y + C_z\mathbf{e}_z$, where C_x, C_y and C_z are the force coefficients in the x, y and z directions, respectively. The coefficients C_x and C_y are shown in figures 3 and 4, respectively. Note that C_y and C_z are primarily determined by the lift force and are similar in nature and smaller in magnitude than C_x which mostly represents the drag force.

The DNS results on C_x and C_y are compared against the estimates using the Schiller-Neumann law based on the instantaneous relative velocity $\mathbf{V}_r$. Also presented in figures 3 and 4 are the estimates that include the inertial (added-mass and pressure gradient) force and the history force, which are also evaluated based on the undisturbed ambient flow at the particle center. For the present case of a stationary particle these additional contributions can be written in dimensional form as

$$\mathbf{F}_{\text{inertial}} = \frac{3}{2} m_f \mathbf{V} \cdot \nabla \mathbf{U} \qquad \text{and} \qquad \mathbf{F}_{\text{history}} = 3d\pi\mu \int_{-\infty}^{t} K(t,\tau)\mathbf{V} \cdot \nabla \mathbf{U} d\tau \,. \quad (14)$$

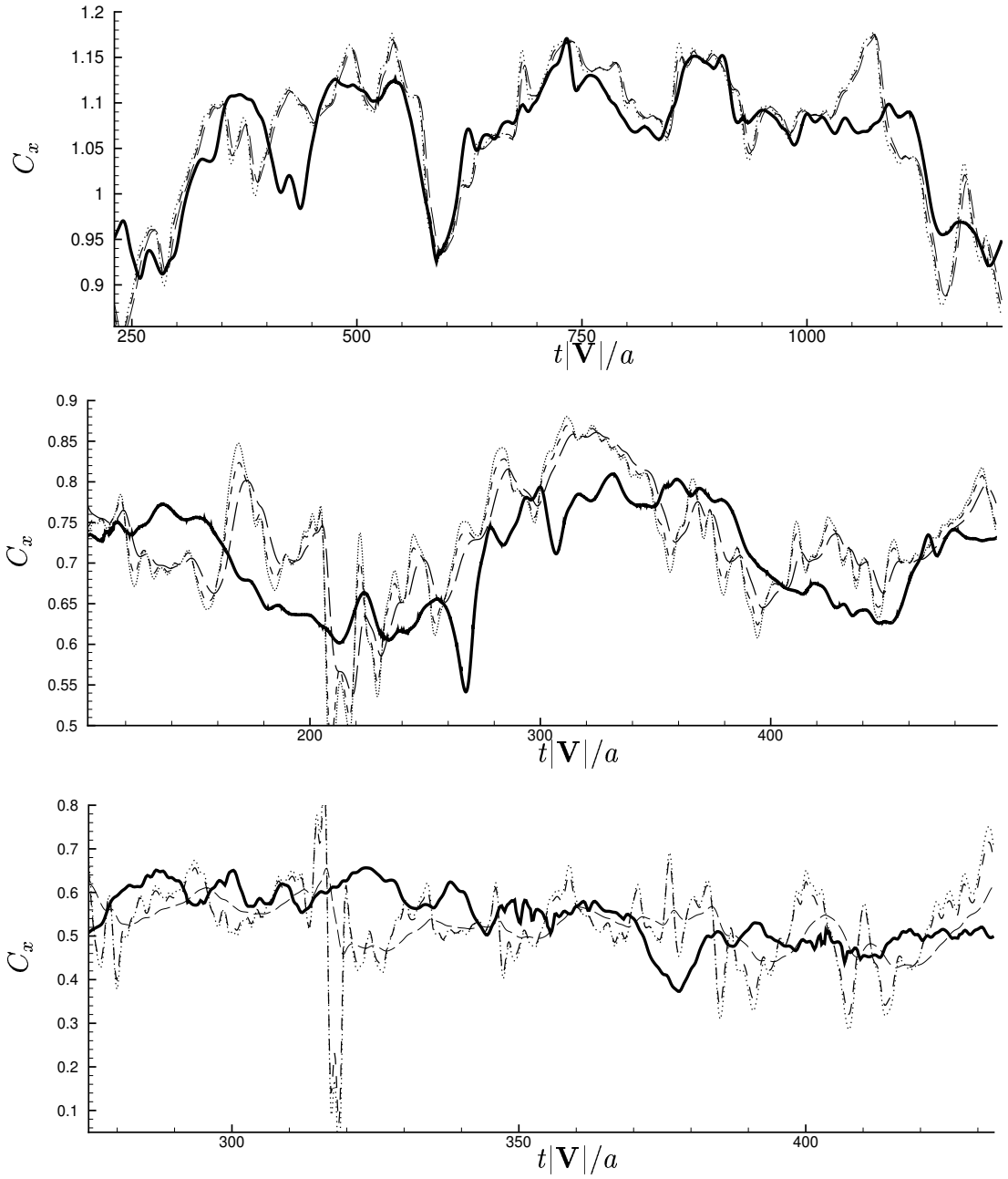

Figure 3: Time history of C_x. Top: case 1 ($d/\eta = 1.5, I = 0.1, \langle Re_r \rangle = 107$), middle: case 3 ($d/\eta = 3.8, I = 0.1, \langle Re_r \rangle = 261$), bottom: case 5 ($d/\eta = 9.6, I = 0.1, \langle Re_r \rangle = 610$). —— DNS result (thick line); — — — Schiller-Neumann law (2); - - - - - - - plus the inertial force; $\cdots\cdots$ plus the history force (14).

The expressions for the inertial and history forces given above correspond to the unsteady undisturbed ambient flow seen by the particle as the isotropic turbulence sweeps past the particle at velocity $\mathbf{V}$. For the history kernel $K(t,\tau)$ the expression given by Mei & Adrian[32] appropriate for moderate Reynolds number is used.

The detailed time-dependence of the drag and lift forces as obtained from the DNS is not precisely reproduced by any of the estimates. For the smallest particle considered (case 1: $d/\eta = 1.5, I = 0.1, \langle Re_r \rangle = 107$), the slow variations in the DNS force are predicted well by the Schiller-Neumann law, whereas the high-frequency fluctuations are not captured. As the particle diameter increases to $d/\eta = 9.59$, the slow variations are no longer accurately predicted by the Schiller-Neumann law. Contribution from the added-mass is quite small for the smallest particle (case 1), but substantially high for the larger particle. Nevertheless, the inclusion of the added-mass force appears to only worsen the prediction by introducing high frequency oscillations (figures 3 and 4). Contribution from the history force, as evaluated by the integral given above, is negligible in all the above cases considered.

The Reynolds number for the $d/\eta = 9.6, I = 0.1$ case is about 610 and therefore the flow in the wake of the particle undergoes natural vortex shedding process. As a result the drag and lift forces for this case are time-dependent even in a nonturbulent uniform ambient flow. The time history of C_x and C_y corresponding to the uniform ambient flow at $\langle Re_r \rangle = 610$ is shown in figure 5. It is interesting to note that the level of fluctuations in C_x in the uniform flow is much lower than that in the turbulent flow. In comparison, the level of fluctuations in C_y is comparable to the

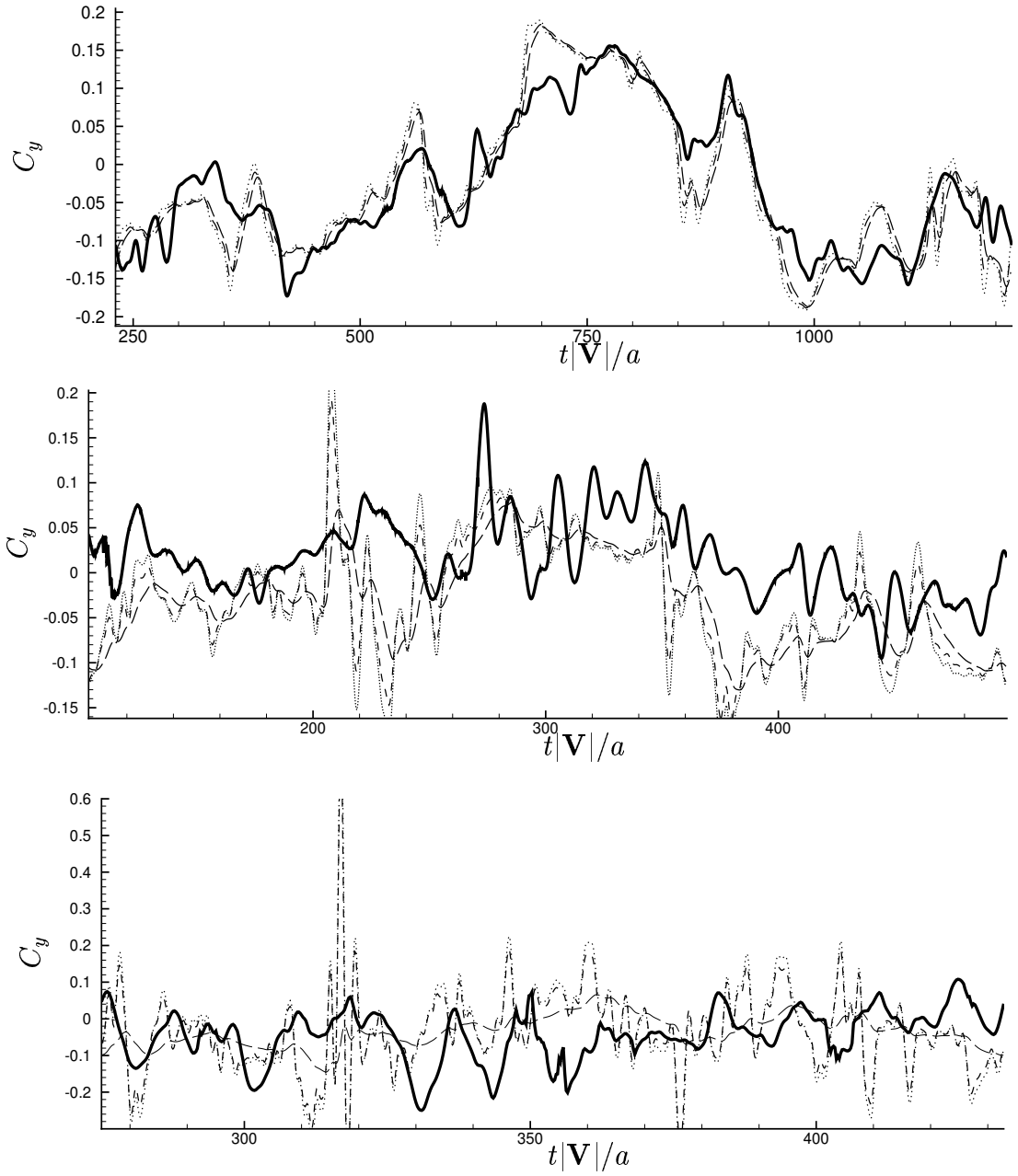

Figure 4: Time history of C_y. Top: case 1 ($d/\eta = 1.5, I = 0.1, \langle Re_r \rangle = 107$), middle: case 3 ($d/\eta = 3.8, I = 0.1, \langle Re_r \rangle = 261$), bottom: case 5 ($d/\eta = 9.6, I = 0.1, \langle Re_r \rangle = 610$). Symbols have the same meaning as in figure 3.

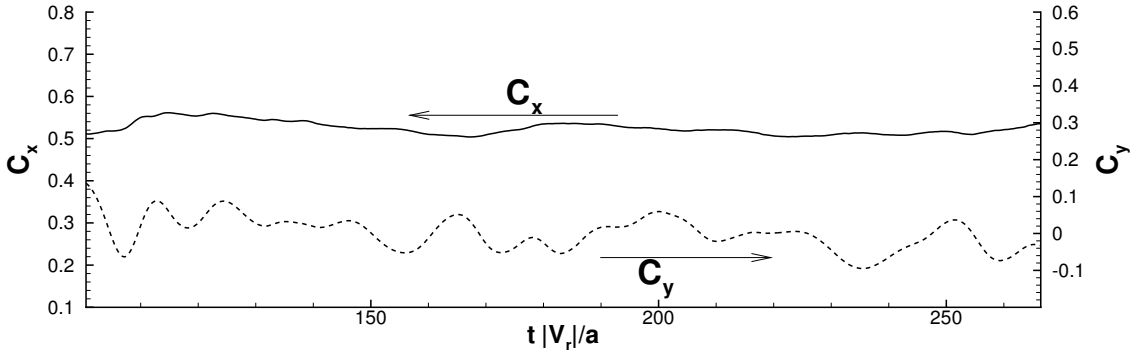

Figure 5: Time history of C_x and C_y for uniform flow corresponding to case 5 ($d/\eta = 9.6, I = 0.1, \langle Re_r \rangle = 610$).

turbulent flow, although some high frequency oscillations can be observed in the case of turbulent flow. Note that in a uniform flow the lift force is generated only due to the vortex shedding process. Freestream turbulence can promote an early onset of vortex shedding. But once the vortex shedding process is established, owing to its absolutely unstable nature, it is only weakly influenced by the freestream turbulence and correspondingly the lift force fluctuates primarily in response to the shedding process with only a weak influence from the freestream turbulence. The drag force, on the other hand, shows substantially enhanced fluctuations in the turbulent flow compared to the uniform flow.

C. Spectra

The spectra of the time-dependent forces corresponding to figures 3 and 4 are shown in figure 6. Here the turbulence intensity is maintained at $I = 0.1$, while d/η increases from 1.5 to 9.6. The spectra of C_x and C_y predicted by the Schiller-

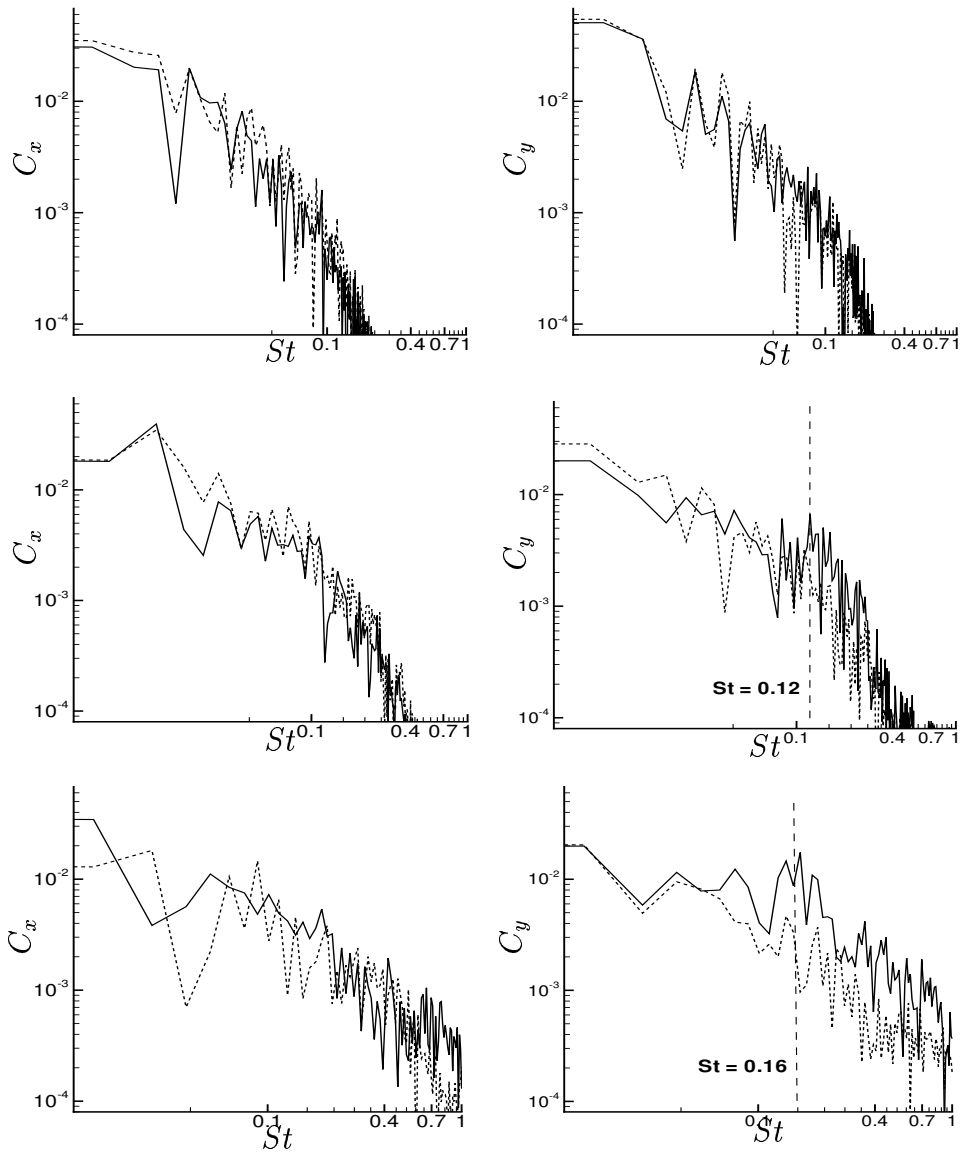

Figure 6: Spectra of C_x (left panel) and C_y (right panel). Top: $d/\eta = 1.5, \langle Re_r \rangle = 107$, middle: $d/\eta = 3.8, \langle Re_r \rangle = 261$, bottom: $d/\eta = 9.6, \langle Re_r \rangle = 610$. For all cases, $I = U_{rms}/|\mathbf{V}| = 0.1$. ——– DNS result; · · · · · · · Schiller-Neumann.

Neumann law applied on an instantaneous basis are also shown along with those of the DNS data. The figures support the observation made earlier that the low frequency component of the DNS data for the smallest particle is well captured by the Schiller-Neumann law applied on an instantaneous basis. At higher frequencies the difference between the DNS data and the Schiller-Neumann prediction increases. For the larger particles, significant difference can be observed in C_x and C_y even at the lowest frequencies. The spectra of C_y (and also C_z) is likely to be influenced the most by the fluctuating lift force, since the flow is dominantly oriented along the x-direction.

For the smallest particle the Reynolds number is sufficiently low and therefore vortex shedding is not expected. The wake only oscillates in response to the freestream turbulence. Thus the spectra of DNS results nearly follow those predicted by the Schiller–Neumann law. For the intermediate particle of size $d/\eta = 3.8$, the Reynolds number $\langle Re_r \rangle = 261$, and in a turbulence-free uniform flow there is no vortex shedding at this Reynolds number. However, the presence of freestream turbulence destabilizes the wake and results in an early initiation of vortex shedding. An extrapolation of the Strouhal number versus Reynolds number curve yields an approximate Strouhal number of about 0.12 at $\langle Re_r \rangle = 261$ (Mittal[17]). Figure 6 shows a modest local peak in the spectra of C_y around this St. For the case of $d/\eta = 9.6, I = 0.1, \langle Re_r \rangle = 610$, the spectra of C_y shows a local peak around $St = 0.16$. The spectra for the uniform flow at this Reynolds number is shown in figure 7, which also shows a local peak in C_y around $St = 0.16$. This is consistent

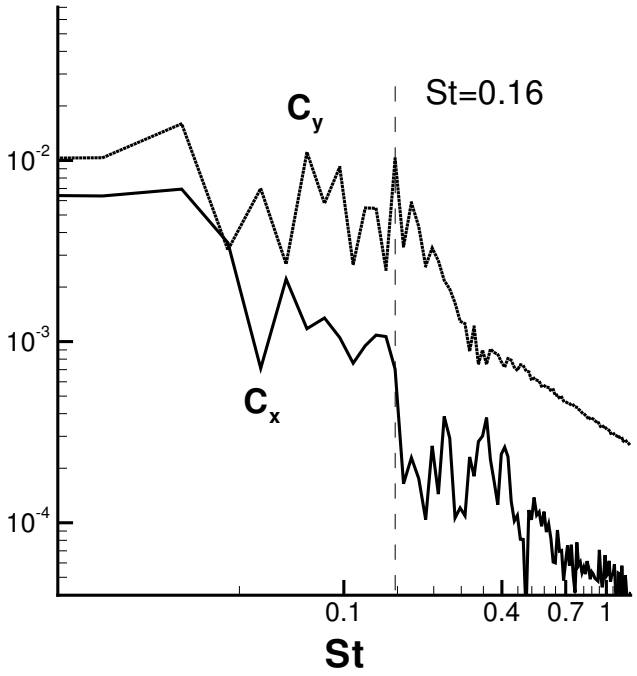

Figure 7: Time history of C_x and C_y for uniform flow corresponding to case 5 ($d/\eta = 9.6, I = 0.1, \langle Re_r \rangle = 610$).

with the previous observation that the lift is not substantially influenced by the freestream turbulence for the largest particle. Also note that the amplitude of high-frequency oscillations is higher in C_y than in C_x for both the uniform and turbulent flows for the largest particle.

D. RMS and cross-correlation

The root-mean-square (rms) of the fluctuations in C_x, C_y, and C_z are shown in figure 8 as a function of the particle size for $I = 0.1$. The rms fluctuations for the

force coefficients are defined as

$$C'_x = \sqrt{\langle (C_x - \langle C_x \rangle)^2 \rangle}\,, \quad C'_y = \sqrt{\langle (C_y - \langle C_y \rangle)^2 \rangle}\,, \quad \text{and} \quad C'_z = \sqrt{\langle (C_z - \langle C_z \rangle)^2 \rangle}\,. \tag{15}$$

In the figure these quantities are scaled by the corresponding freestream velocity fluctuations obtained as

$$U'_x = \sqrt{\langle (U_x - \langle U_x \rangle)^2 \rangle}\,, \quad U'_y = \sqrt{\langle (U_y - \langle U_y \rangle)^2 \rangle}\,, \quad \text{and} \quad U'_z = \sqrt{\langle (U_z - \langle U_z \rangle)^2 \rangle}\,, \tag{16}$$

where $\mathbf{U} = \mathbf{U}(\mathbf{X}_p(t))$ is the instantaneous undisturbed turbulent velocity measured at the center of the particle. The DNS result is compared with the predictions based on the Schiller-Neumann law and with those including the added-mass and the history forces given by (14). For all particle sizes, the prediction using the Schiller-Neumann law appears to be the closest to the DNS result. The effect of including the inertial and history forces is negligible for the smallest particle, and substantial for the largest one. Note that for the smallest particle, the prediction is better for the cross-stream components C'_y and C'_z than for the streamwise component C'_x. For the largest particle (case 5), the reverse is the case. This is because for the smallest particle the cross-stream forces in a uniform flow are zero. In a turbulent flow these forces are entirely induced by the freestream turbulence and hence they tend to closely follow the freestream oscillation. For the largest particle, on the other hand, in an otherwise steady uniform flow unsteady vortex shedding occurs in the wake which generates the fluctuating cross-stream forces. The unsteady vortex shedding persists in the turbulent ambient flow as well resulting in a significant enhancement in the fluctuation of the cross-stream forces.

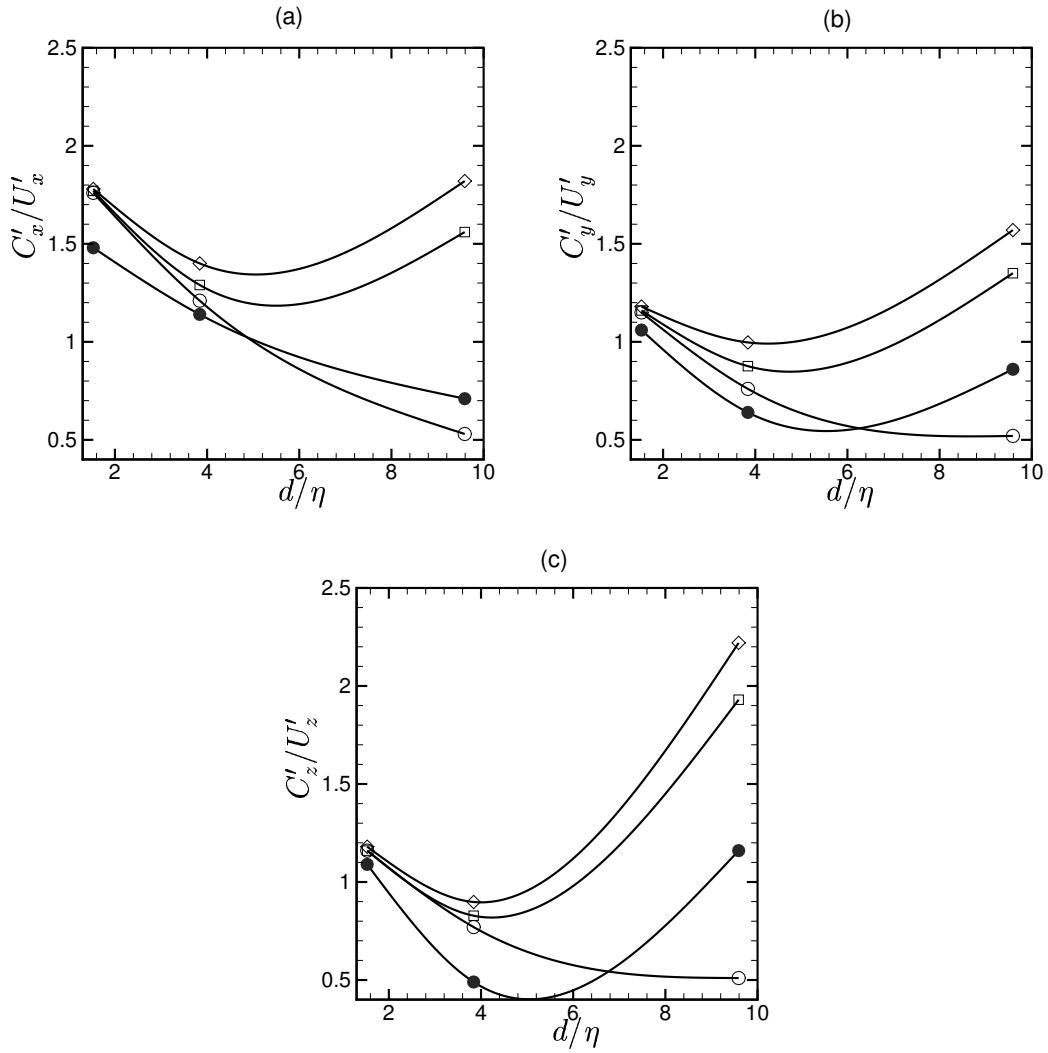

Figure 8: RMS of fluctuations in the force for $I = 0.1$. • DNS, ∘ Schiller-Neumann law (2), □ plus the inertial force, ◇ plus the history force.

In figure 8 it can be observed that for the smallest particle of $d/\eta = 1.5$, the DNS results show that $C'_y/U'_y \approx C'_z/U'_z$. Thus the fluctuations are axisymmetric about the mean wake centerline, as the wake is dominated by the freestream isotropic turbulence. The axisymmetry is however lost at higher $\langle Re_r \rangle$, and C'_y/U'_y considerably differs from C'_z/U'_z. In a uniform ambient flow, at $\langle Re_r \rangle = 610$, there is an approximate plane of symmetry in the wake and the lift force lies on this plane. In a turbulent flow, the shedding process varies with time, and a plane of symmetry is not observed. However, a complete axisymmetry about the wake centerline is not achieved, and hence C'_y/U'_y and C'_z/U'_z are not the same.

It is also interesting to compare the rms fluctuations of the drag and lift forces due to natural vortex shedding in a uniform flow with those in the presence of freestream turbulence. The values of C'_x and C'_y for the uniform and turbulent flow cases for the largest particle $d/\eta = 9.6, I = 0.1, \langle Re_r \rangle = 610$ are 0.015 and 0.059, respectively. Consistent with previous observations, C'_x in the turbulent flow is nearly 4 times that in the uniform flow. In comparison, the values of C'_y for the two cases are 0.044 and 0.064, respectively, and therefore C'_y increases by only a factor of 1.5. Thus the fluctuations in the lift force are dominated by natural vortex shedding, while those in the drag force are substantially influenced by the freestream turbulence.

Cross-correlations between the DNS force and the ambient velocity are shown in table IV. They are computed as

$$\frac{\langle (C_x - \langle C_x \rangle)(U_x - \langle U_x \rangle) \rangle}{C'_x U'_x}, \quad \frac{\langle (C_y - \langle C_y \rangle)(U_y - \langle U_y \rangle) \rangle}{C'_y U'_y}, \tag{17}$$

for the x and y components, and similarly for the z component. For $d/\eta = 1.5$, the

Case	d/η	$I = U_{rms}/\|\mathbf{V}\|$	$\langle Re_r \rangle$	C_x and U_x	C_y and U_y	C_z and U_z
1	1.5	0.1	107	0.852	0.915	0.928
2	1.5	0.2	58	0.842	0.917	0.935
3	3.8	0.1	261	0.634	0.536	0.628
4	3.8	0.25	114	0.488	0.079	0.081
5	9.6	0.1	610	0.258	0.002	0.086
6	9.6	0.25	241	0.13	-0.25	0.079

Table IV: Cross correlation between DNS force and the ambient turbulent velocity.

force response is strongly correlated to the freestream turbulence. The correlation decreases with increasing particle size and also with increasing turbulence intensity. Furthermore, in the case of larger particles, the cross-correlation is much less for the y and z components than for the x components. This is consistent with the previous observation that the lift force for the largest particle is generated due to the vortex shedding precess and not substantially influenced by the freestream turbulence, whereas the drag is strongly influenced by the freestream turbulence.

E. Effect of intensity

The effect of increasing turbulence intensity while keeping the particle diameter fixed is shown in figure 9 for $d/\eta = 1.5$ and in figure 10 for $d/\eta = 9.6$. First of all, as the turbulence intensity (I) increases the mean drag increases, since the corresponding particle Reynolds number decreases as $1/I$. In the figures, the mean is subtracted from the time-dependent force and the fluctuations are presented after scaled by $\langle C_x \rangle I$. The plot for the $d/\eta = 1.5$ case shows that the two cases of $I = 0.1$ and 0.2 yield very similar fluctuations. The similarity of the two results should not be

surprising since for the $I = 0.1$ case the same box of isotropic turbulence is passed over at twise the speed as in the $I = 0.2$ case. For the smallest particle ($d/\eta = 1.5$), the low frequency responses collapse nearly perfectly, however some difference can be observed for the high frequency response. This result is consistent with the discussion given above that for the smallest particle, the drag and lift forces are well correlated with freestream turbulence. Thus the amplitude of fluctuation scales as $\langle C_x \rangle I$, and the scaling appears to be valid for all three components. For the largest particle at $d/\eta = 9.6$, the fluctuations at $I = 0.1$ and 0.25 are not similar. However, the overall intensity of fluctuations still appears to follow the above scaling.

The spectra of the time-dependent force corresponding to figures 9 and 10 are shown in figures 11 and 12, respectively. Similar observation as in the previous figures can be made. For the $d/\eta = 1.5$ case, the frequency response is similar and the amplitude scales as $\langle C_x \rangle I$. For larger particles, however, the responses are dissimilar at different freestream intensities, however, the level of fluctuations follows the above scaling.

The rms of fluctuations in the drag and lift at the higher freestream intensity are shown in figure 13. Again, the rms of the force components are scaled by the corresponding rms of the freestream velocity as defined in (15) and (16). The DNS results show that the rms of C_x increases substantially for all particle sizes. The cross-stream rms, however, does not increase monotonically with d/η. For $d/\eta = 1.5$, both C'_y/U'_y and C'_z/U'_z increase by nearly the same amount. Thus fluctuations in the cross-stream directions are nearly axisymmetric about the wake centerline for

the smallest particle at any freestream intensity. For the intermediate particle at $d/\eta = 3.8$, the rms of the cross-stream fluctuations do not show any substantial change at $I = 0.25$ compared to that at $I = 0.1$. Thus for the intermediate particle, only the drag fluctuations increase. For the largest particle $d/\eta = 9.6$, the rms of cross-stream fluctuations are actually reduced to about 75% of their values at $I = 0.1$. Furthermore, unlike the lower intensity case ($I = 0.1$), the case of higher intensity ($I = 0.25$) shows that C'_y/U'_y and C'_z/U'_z are nearly the same. Thus with increasing freestream intensity the axisymmetric nature of the cross-stream fluctuations is recovered.

The rms fluctuations based on the different estimates are also shown in figure 13. The trend is similar to that observed earlier for the $I = 0.1$ case. The Schiller-Neumann drag is the closest to the DNS results, except however, for the cross-stream fluctuations for the case of $d/\eta = 3.8$ which are substantially reduced compared to the estimate. The inclusion of the added-mass and history forces does not have any substantial effect for $d/\eta = 1.5$ and 3.8, but considerably increases the rms values at $d/\eta = 9.6$ by introducing spurious oscillations.

The rms deviation of the different estimates from the corresponding DNS results is further illustrated by the normalized root-mean-square deviation defined as

$$C''_x = \frac{\langle (C_x - C_{x,DNS})^2 \rangle^{1/2}}{\langle C_{x,DNS} \rangle},$$

$$C''_y = \frac{\langle (C_y - C_{y,DNS})^2 \rangle^{1/2}}{\langle C_{x,DNS} \rangle}, \quad \text{and} \tag{18}$$

$$C_z'' = \frac{\langle (C_z - C_{z,DNS})^2 \rangle^{1/2}}{\langle C_{x,DNS} \rangle}.$$

These quantities are scaled by the freestream turbulence intensity I and shown in figure 14 as a function of the particle size. The figure shows that the rms deviation increases with the particle size and scales with I. It is also clear that the Schiller-Neumann drag law without the inertial and history contributions provides the closest approximation to the DNS results.

F. Estimates for fluid velocity

The use of the undisturbed fluid velocity at the center of the particle as the instantaneous fluid velocity seen by the particle can be questioned. This definition is appropriate for a particle much smaller than the Kolmogorov scale, but for particles of larger size, the definition of the fluid velocity in the various estimates must be reconsidered. A simple approach is to define the instantaneous fluid velocity based on a volume average of the undisturbed ambient flow around the particle. The added-mass and history forces as given in (14) can then be computed using this volume-averaged fluid velocity. The estimates of Schiller-Neumann drag thus computed are plotted in figure 15 for $d/\eta = 1.5, I = 0.1, Re = 107$ (case 1) for two different approximations of the fluid velocity seen by the particle: one obtained by averaging the undisturbed fluid over a volume of 2 times the particle diameter and the other obtained by averaging over 10 times the particle diameter. Also plotted for comparison are the DNS data and estimates that include the inertial and history contributions based on the volume-averaged fluid velocity. The results for case 5

$(d/\eta = 9.6, I = 0.1, Re = 610)$ using averaging volumes of size 1.2 and 10 times the particle diameter are shown in figure 16.

Expectedly, with increasing size of the volume of averaging, the time variation in the estimated force decreases. In particular, the high frequency components are significantly diminished. As a result the inertial and history contributions are also suppressed. For the different cases shown the mean drag remains virtually unaffected by the size of the averaging volume (table V). Of course, in the limit when the volume of averaging becomes as large as the box of turbulence the fluid velocity seen by the particle becomes a constant equal to $\mathbf{V}$ and the corresponding drag estimate reduces to (12), resulting in a substantially different estimation of the mean drag (see estimate 3 in table III).

The rms fluctuation of C_x and C_y obtained by using the above volume-averaged estimates are shown in figure 17 as a function of the size of the averaging volume. The rms fluctuations are computed using (15). The rms of the DNS result is also shown. For the smallest particle the comparison of the rms fluctuation with the DNS data improves as the size of the averaging volume increases. However, for the larger particles, the rms fluctuation in the Schiller-Neumann estimation is lower than the DNS result even when the fluid velocity is taken to be at the center of the particle. With increasing size of the averaging volume the rms fluctuation in the Schiller-Neumann estimation further decreases. Note that the larger particle is about 6.5 times bigger than the smaller particle. The inclusion of the inertial and history forces increases the level of fluctuation, however, these fluctuations do

	$1.2d$	$10d$
Schiller-Neumann	0.532	0.529
Schiller-Neumann + Inertial force	0.532	0.529
Schiller-Neumann + Inertial force + History force	0.529	0.529

Table V: Mean drag by using different volume-averaged estimates for the fluid velocity. $d/\eta = 9.6, I = 0.1, \langle Re_r \rangle = 610$ (case 5). Mean drag is unaffected by the estimates and by addition of the added-mass and history forces based on those estimates.

not necessarily reflect the actual behavior. With increasing size of the averaging volume these fluctuations diminish, and the difference from the Schiller-Neumann estimation decreases. This fact is illustrated by computing the rms deviation in the different estimates from the corresponding true DNS results as given in (18). These results as a function of the size of the averaging volume for two different cases are shown in figure 18. It is clear that the Schiller-Neumann drag law without the inertial and history contributions provides the closest approximation to the DNS results.

IV. Summary and conclusion

The purpose of this paper is to address the effect of freestream turbulence on the drag force on a particle. We consider direct numerical simulation of a particle subjected to a frozen isotropic turbulent flow. The particle Reynolds number is about 50 to 600, the diameter is about 1.5 to 10 times the Kolmogorov scale, and

the freestream turbulence intensity is about 10 to 25%. We compare the DNS results on the mean and time-dependent drag with the predictions based on the standard drag correlation, and those including the added-mass and history forces.

We observe that the freestream turbulence does not have a systematic and substantial effect on the mean drag. The standard drag correlation based on the instantaneous or mean slip velocity yields a reasonably accurate prediction of the mean drag obtained from the DNS. The mean drag however depends on the definition of the mean fluid velocity. The mean fluid velocity obtained by averaging over the entire volume of fluid can result in a significantly different value of the mean drag if the particle does not sample the entire volume.

The accuracy of prediction of the instantaneous drag force decreases with increasing particle size. For the smallest particle, the low frequency oscillations in the DNS drag are well captured by the standard drag, but for the larger particles significant differences exist even for the low frequency components. For the smallest particle, the cross-correlation between the DNS drag and the freestream velocity is the highest, and it decreases with increasing particle size.

Inclusion of the added-mass and history forces does not improve the prediction, and for the larger particles these forces introduce spurious oscillations not observed in the DNS. Analysis of the rms fluctuations suggests that the standard drag correlation provides the closest approximation for the DNS results.

The fluctuations in the cross-stream forces are statistically axisymmetric about the wake centerline for the smallest particle but not for the larger particles, where

vortex shedding begins to play a role. For the largest particle, the effect of freestream turbulence is strong on the streamwise force than on the cross-stream forces, which are dominated by natural vortex shedding. The cross-stream forces become axisymmetric as the freestream intensity increases, which begins to suppress natural vortex shedding.

We observe the magnitude of fluctuations in the drag and lift forces to scale linearly with both the mean drag and freestream turbulence intensity, i.e., $C_x', C_y', C_z' \propto I(1 + 0.15\, Re^{0.687})\, Re^{-1}$.

Since the use of the undisturbed fluid velocity measured at the center of the particle as the fluid velocity seen by the particle is *ad hoc*, we examine various approximations to the fluid velocity obtained by averaging over a volume of fluid around the particle. It is shown that the mean drag is insensitive to the definition of the mean fluid velocity, as far as the latter is defined either based on the undisturbed fluid velocity at the center of the particle, or based on an estimate obtained by averaging over a fluid volume of the order of the particle size. The fluctuations diminish as the volume of averaging increases. The overall conclusion is that the standard drag correlation without the added-mass and history forces provides the closest approximation to the DNS result.

ACKNOWLEDGEMENT

The research is supported by the ASCI Center for Simulation of Advanced Rockets at the University of Illinois at Urbana-Champaign through the U.S. Department

of Energy (B341494). Computational facilities from the National Center for Supercomputing Applications, UIUC are greatly acknowledged. Thanks are also due to Drs. J.P. Ferry and F.M. Najjar.

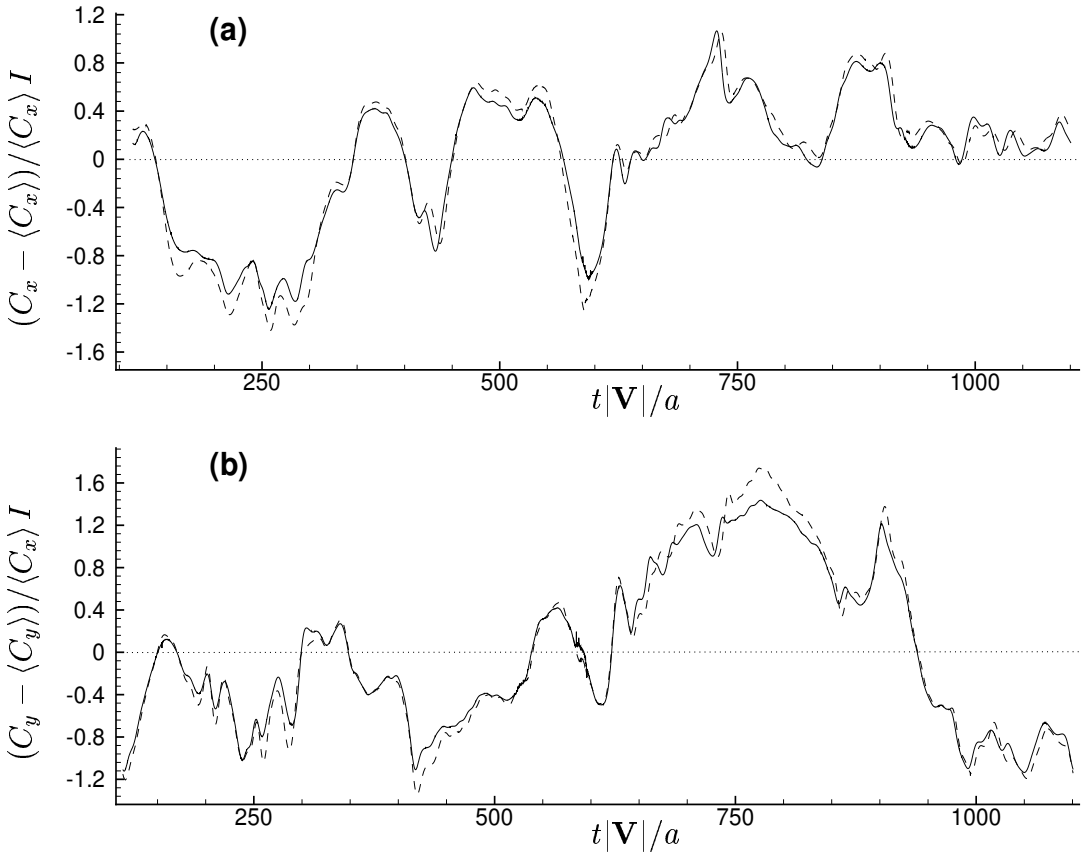

Figure 9: Effect of increasing freestream turbulence intensity while the particle size is fixed at $d/\eta = 1.5$. —— $I = 0.2$; - - - - - - $I = 0.1$. (a) $(C_x - \langle C_x \rangle)/\langle C_x \rangle\, I$, (b) $(C_y - \langle C_y \rangle)/\langle C_x \rangle\, I$.

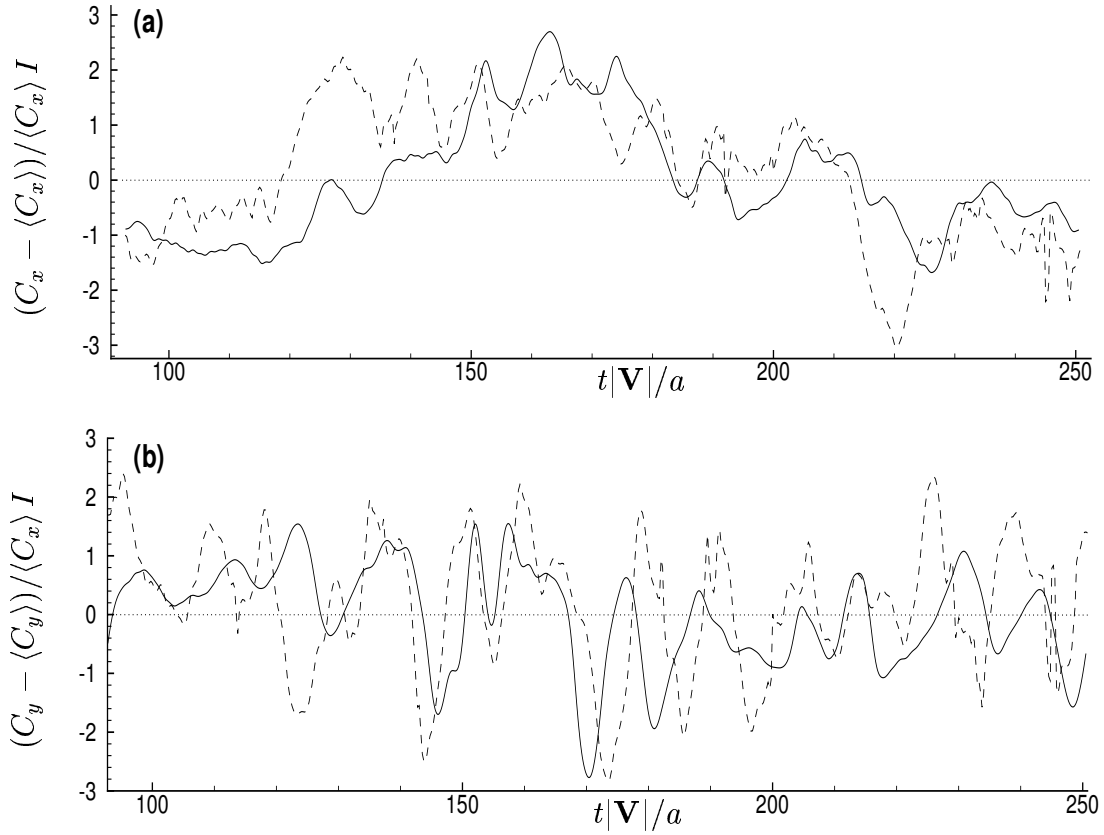

Figure 10: Effect of increasing freestream turbulence intensity while the particle size is fixed at $d/\eta = 9.6$. —— $I = 0.25$; - - - - - - $I = 0.1$. (a) $(C_x - \langle C_x \rangle)/\langle C_x \rangle I$, (b) $(C_y - \langle C_y \rangle)/\langle C_x \rangle I$.

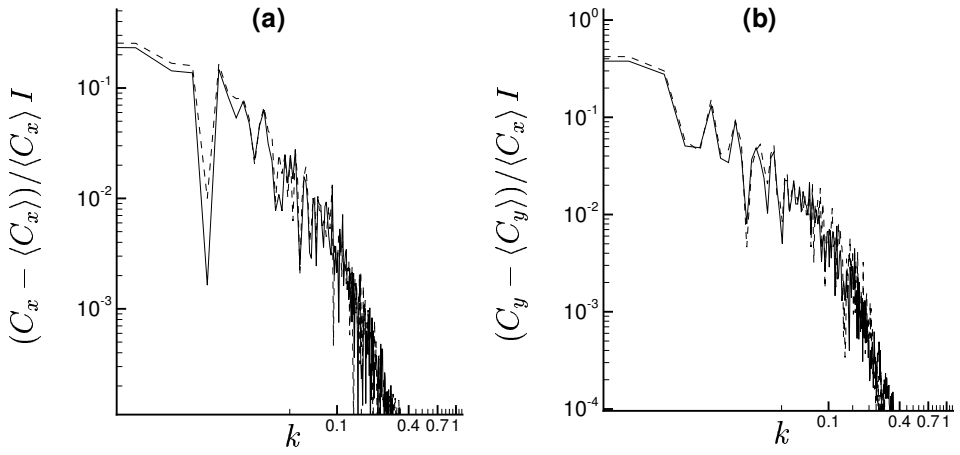

Figure 11: Effect of increasing turbulence intensity at the same particle size. Spectra corresponding to figure 9 for $d/\eta = 1.5$. Symbols have the same meaning as in fig. 9.

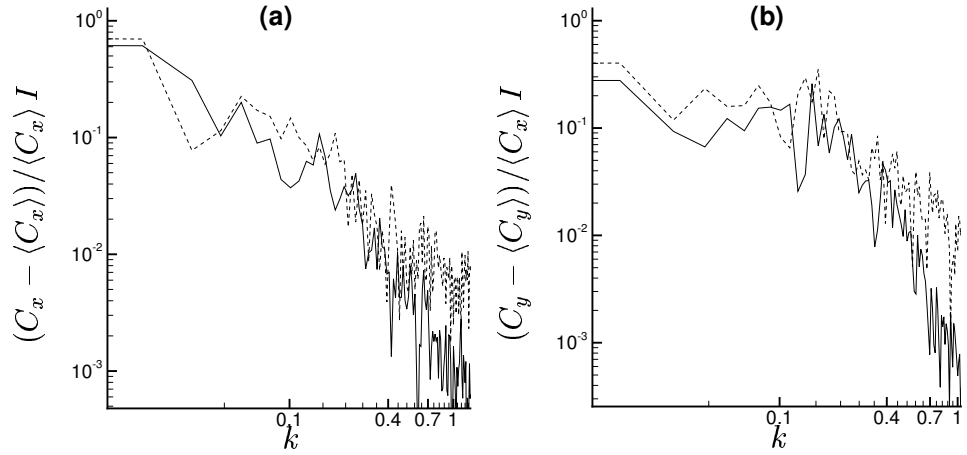

Figure 12: Effect of increasing turbulence intensity at the same particle size. Spectra corresponding to figure 10 for $d/\eta = 9.6$. Symbols have the same meaning as in fig. 10.

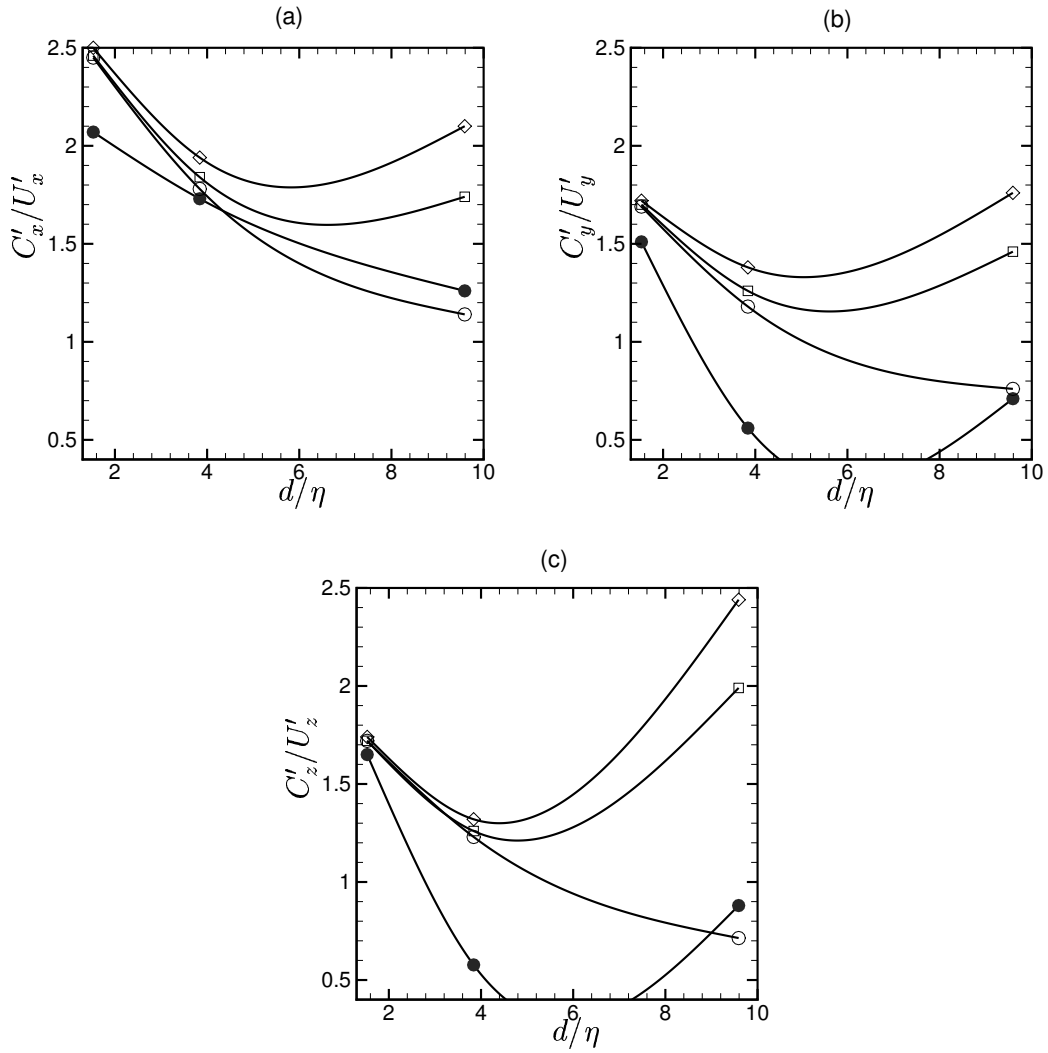

Figure 13: RMS of fluctuations in the force for $I = 0.2$ or $I = 0.25$. • DNS, ◦ Schiller-Neumann law (2), □ plus the inertial force, ◇ plus the history force.

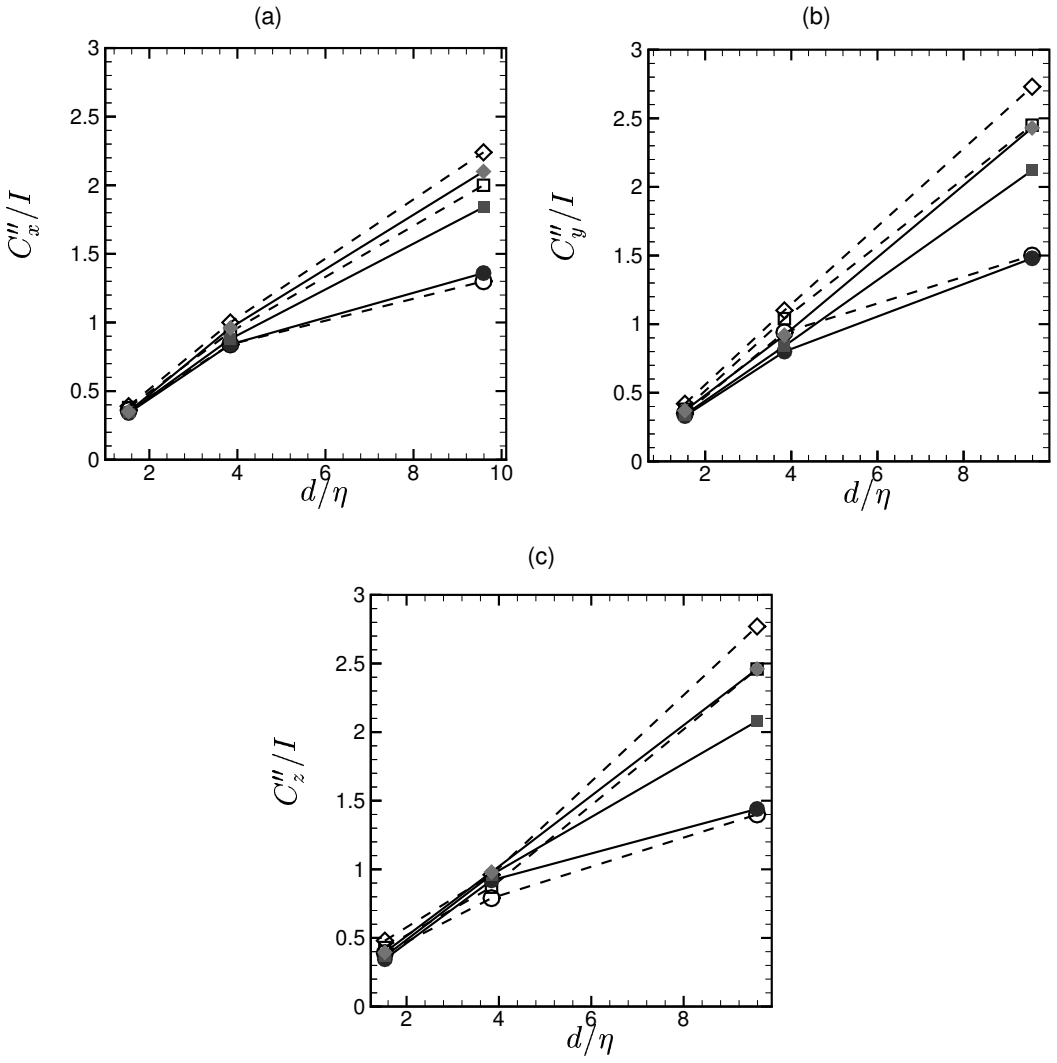

Figure 14: Root-mean-square deviation of the DNS results from the predictions scaled by the freestream turbulence intensity. ∘ Schiller-Neumann law, □ plus the inertial force, ◇ plus the history force. The dashed lines and open symbols are for $I = 0.1$, and the thick lines and solid symbols are for $I = 0.2$ or $I = 0.25$.

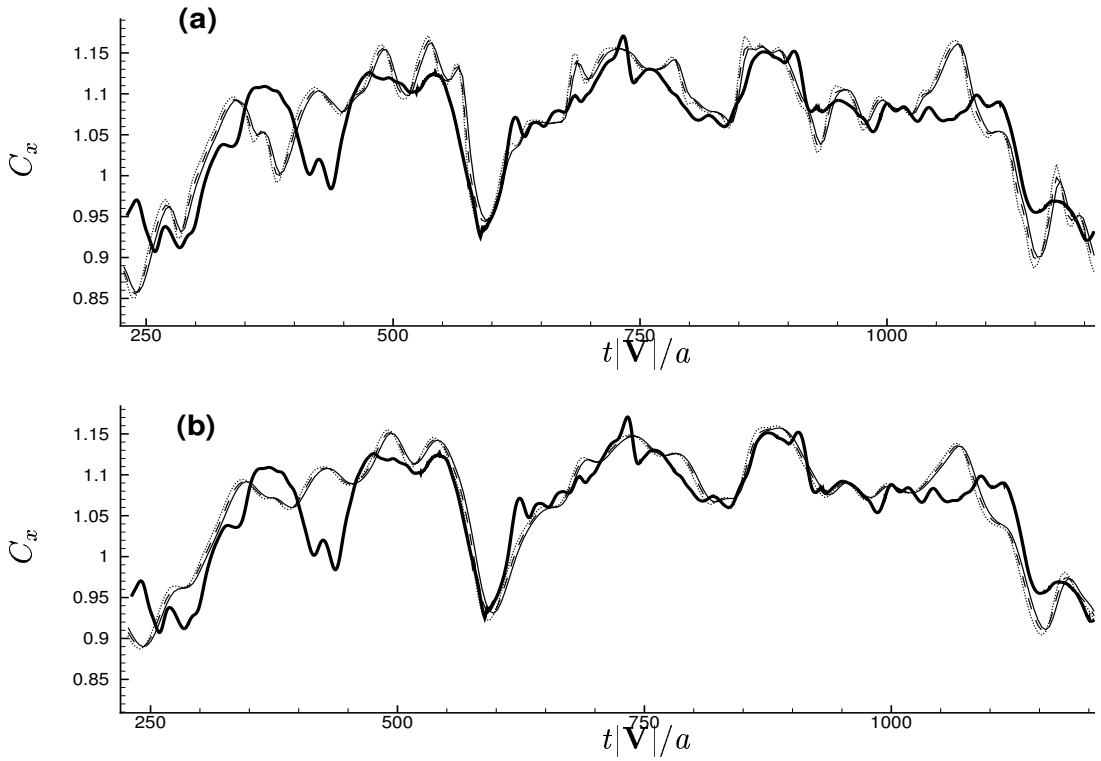

Figure 15: C_x. $d/\eta = 1.5, I = 0.1$. Top: 2d average, bottom: 10d average. Thick line is the DNS result. —— Schiller-Neumann drag, - - - - - - with inertial force, · · · · · with history force.

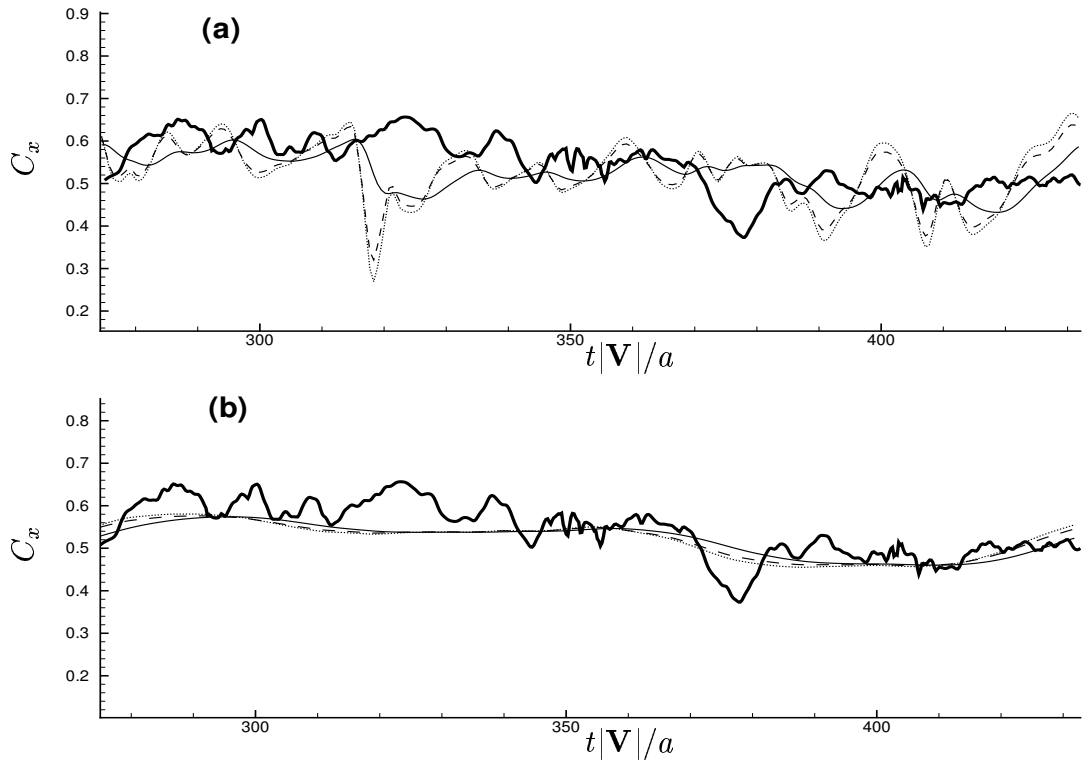

Figure 16: C_x. $d/\eta = 9.6$. Top: $1.2d$ average, bottom: 10d average. Symbols have same meaning as in figure 15.

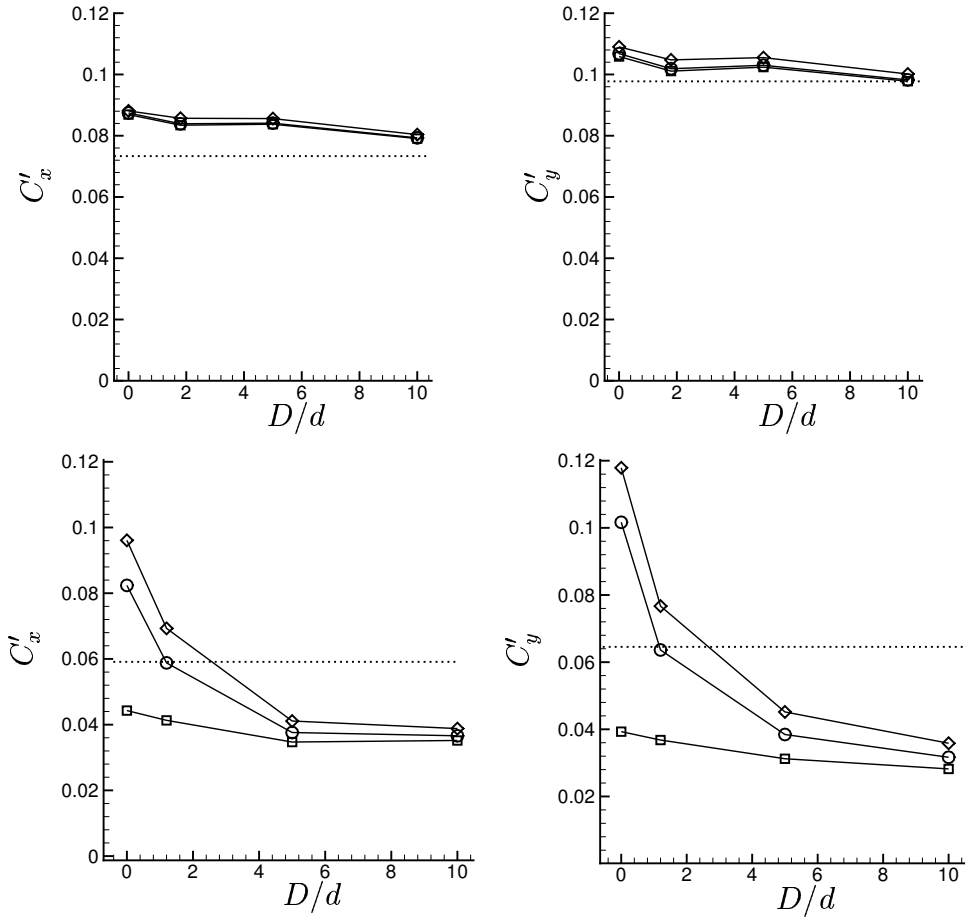

Figure 17: RMS of C_x (left panel) and C_y (right panel) based on different volume-averaged estimates for the fluid velocity. D is the diameter of the volume of averaging. Top : $d/\eta = 1.5, I = 0.1, \langle Re_r \rangle = 107$; bottom: $d/\eta = 9.6, I = 0.1, \langle Re_r \rangle = 610$. The dotted line indicates the DNS result. $\square$ Schiller-Neumann; $\circ$ with inertial force; $\diamond$ with inertial and history force. $D/d = 0$ indicates the undisturbed fluid velocity measured at the center of the particle.

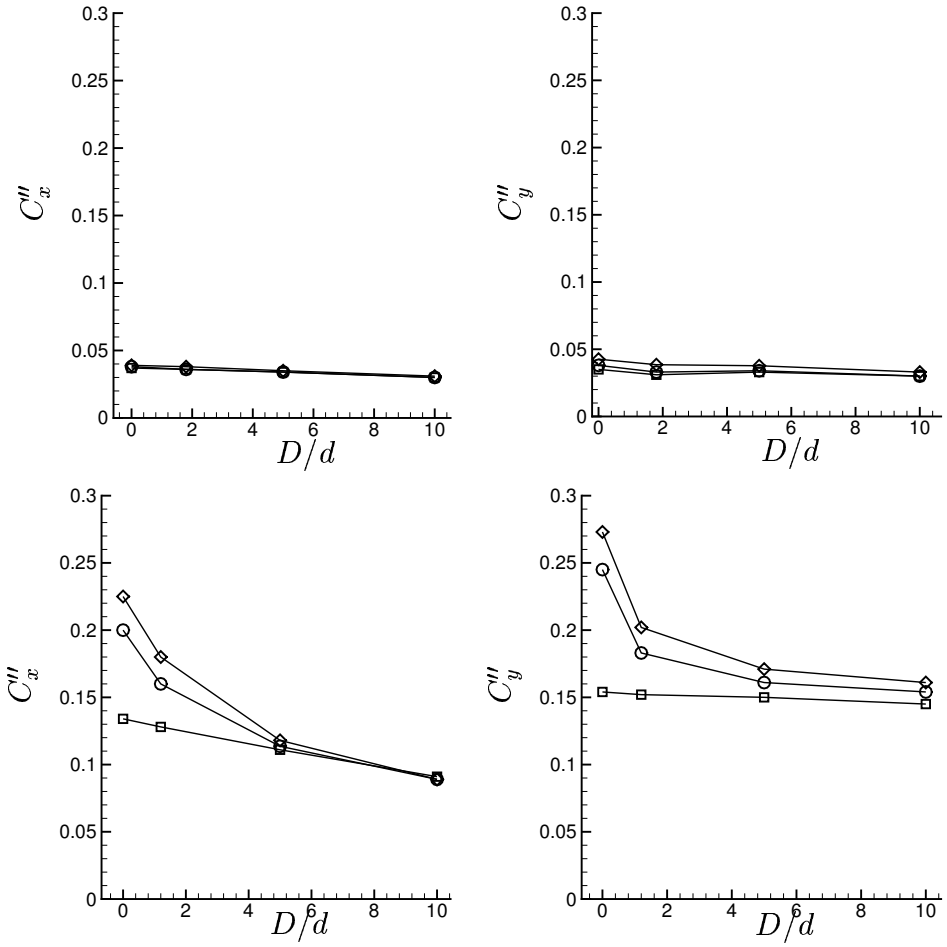

Figure 18: Root mean square deviation from the DNS results of predictions using different volume-averaged estimates for fluid velocity. Top : $d/\eta = 1.5, I = 0.1, \langle Re_r \rangle = 107$; bottom: $d/\eta = 9.6, I = 0.1, \langle Re_r \rangle = 610$. Symbols: $\square$ Schiller-Neumann; $\circ$ with inertial force; $\diamond$ with the inertial and history forces.

References

[1] Mei, R., Adrian, R. J., & Hanratty, T. J. 1991 Particle dispersion in isotropic turbulence under Stokes drag and Basset force with gravitational settling. *Journal of Fluid Mechanics* **225**, 481–495.

[2] Wang, L.-P., & Maxey, M. R. 1993 Settling velocity and concentration distribution of heavy particles in homogeneous isotropic turbulence. *Journal of Fluid Mechanics.* **256**, 27–68.

[3] Uhlherr, P. H. T., & Sinclair, C. G. 1970 The effect of freestream turbulence on the drag coefficients of spheres. *Proceeding of Chemca.* **1**, 1–12.

[4] Zarin, N. A., & Nicholls, J. A. 1971 Sphere drag in solid rockets—noncontinuum and turbulence effects. *Combustion Science and Technology* **3**, 273–280.

[5] Brucato, A., Grisafi, F., & Montante, G. 1998 Particle drag coefficients in turbulent fluids. *Chem. Eng. Sc.*, **53**, 3295–3314.

[6] Yusof, J. 1996 Interaction of massive particles with turbulence. PhD Thesis, Department of Mechanical Engineering, Cornell University.

[7] Rudolff, R. R. & Bachalo, W. D. 1988 Measurement of droplet drag coefficients in polydispersed turbulent flow field. AIAA paper, 88-0235.

[8] Warnica, W. D., Renksizbulut, M., & Strong, A. B. 1994 Drag coefficient of spherical liquid droplets. *Experiments in Fluids* **18**, 265–270.

[9] Wu, J.-S., & Faeth, G. M. 1994a Sphere wakes at moderate Reynolds numbers in a turbulent environment. *AIAA Journal* **32**, 535–541.

[10] Wu, J.-S., & Faeth, G. M. 1994b Effect of ambient turbulence intensity on sphere wakes at intermediate Reynolds numbers. *AIAA Journal* **33**, 171–173.

[11] Torobin, L. B., & Gauvin, W. H. 1959 Fundamental aspects of solid–gas flow: Part 1. *Canadian Journal of Chemical Engineering* **38**, 129–141.

[12] Torobin, L. B., & Gauvin, W. H. 1961 Drag coefficients of single spheres moving in steady and accelerated motion in a turbulent fluid. *American Institute of Chemical Engineers Journal* **7**, 615–620.

[13] Clamen, A. & Gauvin, W. H. 1969 Effect of turbulence on the drag coefficients of spheres in a supercritical flow regime. *AIChE J.*, **15**, 184.

[14] Clift, R. & Gauvin, W. H. 1970 The motion of particles in turbulent gas streams. *Proc. Chemca*, **1**, 14.

[15] Gore, R. A. & Crowe, C. T. 1990 Discussion of "Particle drag in a dilute turbulent two-phase suspension flow". *Int. J. Multiphase Flow*, **16**, 359–361.

[16] Sankagiri, S. & Ruff, G. A. 1997 Measurement of sphere drag in high turbulent intensity flows. Proc. ASME Fluids Engineering Division, FED-Vol 244, 277–282.

[17] Mittal, R. 2000 Response of the sphere wake to freestream fluctuations. *Theoretical and Computational Fluid Dynamics*, **13**, 397–419.

[18] Clift, R., Grace, J. R., & Weber, M. E. 1978 *Bubbles, Drops and Particles.* Academic.

[19] Langford, J. A. 2000 Toward ideal larger-eddy simulation. PhD Thesis, Department of Theoretical and Applied Mechanics, University of Illinois at Urbana-Champaign, Urbana, Ill.

[20] Bagchi, P. & Balachandar, S. 2002 Steady planar straining flow past a rigid sphere at moderate Reynolds number. *Journal of Fluid Mechanics* **466**, 365–407.

[21] Mittal, R., & Balachandar, S. 1996 Direct numerical simulation of flow past elliptic cylinders. *Journal Computational Physics* **124**, 351–367.

[22] Tsuju, Y., Morikawa, Y., & Shiomi, H. 1984 LDV measurement of an air-solid two-phase flow in a vertical pipe. *Journal of Fluid Mechanics* **139**, 417–434.

[23] Mizukami, M., Parthasarathy, R. N., & Faeth, G. M. 1992 Particle generated turbulence in homogeneous dilute dispersed flow. *International Journal of Multiphase Flow* **18**, 397–412.

[24] Parthasarathy R. N., & Faeth G. M. 1990 Turbulence modulation in homogeneous dilute particle-laden flows. *Journal of Fluid Mechanics* **220**, 485–514.

[25] Chen, J. -H., & Faeth, G. M. 2000 Continuous-phase properties of homogeneous particle-laden turbulent flows. *AIAA Journal* **39**, 180–183.

[26] Chen, J. -H., Wu, J. -S., & Faeth, G. M. 2000 Turbulence generation in homogeneous particle-laden flows. *AIAA Journal* **38**, 636–642.

[27] Kulick, J. D., Fessler, J. R., & Eaton, J. K. 1994 Particle response and turbulence modification in fully developed channel flow. *Journal of Fluid Mechanics* **277**, 109–134.

[28] Longmire E. K., & Eaton J. K. 1992 Structure of a particle-laden round jet. *Journal of Fluid Mechanics* **236**, 217–257.

[29] Pan, Y. & Bannerjee, S. 1997 Numerical investigation of the effects of large particles on wall turbulence. *Physics of Fluids*, **9**, 3786–3807.

[30] Schiller, L., & Neumann, A. 1933 Uber die grundlegenden Berechungen bei der Schwer kraftaufbereitung. *Verein Deutscher Ingenieure* **77**, 318–324.

[31] Tsuji Y., Morikawa Y., Tanaka T., Karimine K., & Nishida S. 1988 Measurement of an axisymmetric jet laden with coarse particles. *Int. J. Multiphase Flow* **14**, 565–574.

[32] Mei, R. & Adrian, R. J. 1992 Flow past a sphere with an oscillation in the free-stream and unsteady drag at finite Reynolds number. *J. Fluid Mech.* **237**, 133–174.

List of Recent TAM Reports

No.	*Authors*	*Title*	*Date*
927	Ferry, J. P., and S. Balachandar	A fast Eulerian method for two-phase flow—*International Journal of Multiphase Flow*, in press (2000)	Feb. 2000
928	Thoroddsen, S. T., and K. Takehara	The coalescence–cascade of a drop—*Physics of Fluids* **12**, 1257–1265 (2000)	Feb. 2000
929	Liu, Z.-C., R. J. Adrian, and T. J. Hanratty	Large-scale modes of turbulent channel flow: Transport and structure—*Journal of Fluid Mechanics* **448**, 53–80 (2001)	Feb. 2000
930	Borodai, S. G., and R. D. Moser	The numerical decomposition of turbulent fluctuations in a compressible boundary layer—*Theoretical and Computational Fluid Dynamics* (submitted)	Mar. 2000
931	Balachandar, S., and F. M. Najjar	Optimal two-dimensional models for wake flows—*Physics of Fluids*, in press (2000)	Mar. 2000
932	Yoon, H. S., K. V. Sharp, D. F. Hill, R. J. Adrian, S. Balachandar, M. Y. Ha, and K. Kar	Integrated experimental and computational approach to simulation of flow in a stirred tank—*Chemical Engineering Sciences* **56**, 6635–6649 (2001)	Mar. 2000
933	Sakakibara, J., Hishida, K., and W. R. C. Phillips	On the vortical structure in a plane impinging jet—*Journal of Fluid Mechanics* **434**, 273–300 (2001)	Apr. 2000
934	Phillips, W. R. C.	Eulerian space–time correlations in turbulent shear flows—*Physics of Fluids* **12**, 2056–2064 (2000)	Apr. 2000
935	Hsui, A. T., and D. N. Riahi	Onset of thermal–chemical convection with crystallization within a binary fluid and its geological implications—*Geochemistry, Geophysics, Geosystems* **2**, 2000GC000075 (2001)	Apr. 2000
936	Cermelli, P., E. Fried, and S. Sellers	Configurational stress, yield, and flow in rate-independent plasticity—*Proceedings of the Royal Society of London A* **457**, 1447–1467 (2001)	Apr. 2000
937	Adrian, R. J., C. Meneveau, R. D. Moser, and J. J. Riley	Final report on 'Turbulence Measurements for Large-Eddy Simulation' workshop	Apr. 2000
938	Bagchi, P., and S. Balachandar	Linearly varying ambient flow past a sphere at finite Reynolds number—Part 1: Wake structure and forces in steady straining flow	Apr. 2000
939	Gioia, G., A. DeSimone, M. Ortiz, and A. M. Cuitiño	Folding energetics in thin-film diaphragms—*Proceedings of the Royal Society of London A* **458**, 1223–1229 (2002)	Apr. 2000
940	Chaïeb, S., and G. H. McKinley	Mixing immiscible fluids: Drainage induced cusp formation	May 2000
941	Thoroddsen, S. T., and A. Q. Shen	Granular jets—*Physics of Fluids* **13**, 4–6 (2001)	May 2000
942	Riahi, D. N.	Non-axisymmetric chimney convection in a mushy layer under a high-gravity environment—In *Centrifugal Materials Processing* (L. L. Regel and W. R. Wilcox, eds.), 295–302 (2001)	May 2000
943	Christensen, K. T., S. M. Soloff, and R. J. Adrian	PIV Sleuth: Integrated particle image velocimetry interrogation/validation software	May 2000
944	Wang, J., N. R. Sottos, and R. L. Weaver	Laser induced thin film spallation—*Experimental Mechanics* (submitted)	May 2000
945	Riahi, D. N.	Magnetohydrodynamic effects in high gravity convection during alloy solidification—In *Centrifugal Materials Processing* (L. L. Regel and W. R. Wilcox, eds.), 317–324 (2001)	June 2000
946	Gioia, G., Y. Wang, and A. M. Cuitiño	The energetics of heterogeneous deformation in open-cell solid foams—*Proceedings of the Royal Society of London A* **457**, 1079–1096 (2001)	June 2000

List of Recent TAM Reports (cont'd)

No.	Authors	Title	Date
947	Kessler, M. R., and S. R. White	Self-activated healing of delamination damage in woven composites—*Composites A: Applied Science and Manufacturing* **32**, 683–699 (2001)	June 2000
948	Phillips, W. R. C.	On the pseudomomentum and generalized Stokes drift in a spectrum of rotational waves—*Journal of Fluid Mechanics* **430**, 209–229 (2001)	July 2000
949	Hsui, A. T., and D. N. Riahi	Does the Earth's nonuniform gravitational field affect its mantle convection?—*Physics of the Earth and Planetary Interiors* (submitted)	July 2000
950	Phillips, J. W.	Abstract Book, 20th International Congress of Theoretical and Applied Mechanics (27 August – 2 September, 2000, Chicago)	July 2000
951	Vainchtein, D. L., and H. Aref	Morphological transition in compressible foam—*Physics of Fluids* **13**, 2152–2160 (2001)	July 2000
952	Chaïeb, S., E. Sato-Matsuo, and T. Tanaka	Shrinking-induced instabilities in gels	July 2000
953	Riahi, D. N., and A. T. Hsui	A theoretical investigation of high Rayleigh number convection in a nonuniform gravitational field—*Acta Mechanica* (submitted)	Aug. 2000
954	Riahi, D. N.	Effects of centrifugal and Coriolis forces on a hydromagnetic chimney convection in a mushy layer—*Journal of Crystal Growth* **226**, 393–405 (2001)	Aug. 2000
955	Fried, E.	An elementary molecular-statistical basis for the Mooney and Rivlin–Saunders theories of rubber-elasticity—*Journal of the Mechanics and Physics of Solids* **50**, 571–582 (2002)	Sept. 2000
956	Phillips, W. R. C.	On an instability to Langmuir circulations and the role of Prandtl and Richardson numbers—*Journal of Fluid Mechanics* **442**, 335–358 (2001)	Sept. 2000
957	Chaïeb, S., and J. Sutin	Growth of myelin figures made of water soluble surfactant—Proceedings of the 1st Annual International IEEE–EMBS Conference on Microtechnologies in Medicine and Biology (October 2000, Lyon, France), 345–348	Oct. 2000
958	Christensen, K. T., and R. J. Adrian	Statistical evidence of hairpin vortex packets in wall turbulence—*Journal of Fluid Mechanics* **431**, 433–443 (2001)	Oct. 2000
959	Kuznetsov, I. R., and D. S. Stewart	Modeling the thermal expansion boundary layer during the combustion of energetic materials—*Combustion and Flame*, in press (2001)	Oct. 2000
960	Zhang, S., K. J. Hsia, and A. J. Pearlstein	Potential flow model of cavitation-induced interfacial fracture in a confined ductile layer—*Journal of the Mechanics and Physics of Solids*, **50**, 549–569 (2002)	Nov. 2000
961	Sharp, K. V., R. J. Adrian, J. G. Santiago, and J. I. Molho	Liquid flows in microchannels—Chapter 6 of *CRC Handbook of MEMS* (M. Gad-el-Hak, ed.) (2001)	Nov. 2000
962	Harris, J. G.	Rayleigh wave propagation in curved waveguides—*Wave Motion* **36**, 425–441 (2002)	Jan. 2001
963	Dong, F., A. T. Hsui, and D. N. Riahi	A stability analysis and some numerical computations for thermal convection with a variable buoyancy factor—*Journal of Theoretical and Applied Mechanics*, in press (2002)	Jan. 2001
964	Phillips, W. R. C.	Langmuir circulations beneath growing or decaying surface waves—*Journal of Fluid Mechanics* (submitted)	Jan. 2001
965	Bdzil, J. B., D. S. Stewart, and T. L. Jackson	Program burn algorithms based on detonation shock dynamics—*Journal of Computational Physics* (submitted)	Jan. 2001
966	Bagchi, P., and S. Balachandar	Linearly varying ambient flow past a sphere at finite Reynolds number: Part 2—Equation of motion—*Journal of Fluid Mechanics* (submitted)	Feb. 2001
967	Cermelli, P., and E. Fried	The evolution equation for a disclination in a nematic fluid—*Proceedings of the Royal Society A* **458**, 1–20 (2002)	Apr. 2001

List of Recent TAM Reports (cont'd)

No.	Authors	Title	Date
968	Riahi, D. N.	Effects of rotation on convection in a porous layer during alloy solidification—Chapter 12 in *Transport Phenomena in Porous Media* (D. B. Ingham and I. Pop, eds.), 316–340 (2002)	Apr. 2001
969	Damljanovic, V., and R. L. Weaver	Elastic waves in cylindrical waveguides of arbitrary cross section—*Journal of Sound and Vibration* (submitted)	May 2001
970	Gioia, G., and A. M. Cuitiño	Two-phase densification of cohesive granular aggregates—*Physical Review Letters* **88**, 204302 (2002) (in extended form and with added co-authors S. Zheng and T. Uribe)	May 2001
971	Subramanian, S. J., and P. Sofronis	Calculation of a constitutive potential for isostatic powder compaction—*International Journal of Mechanical Sciences* (submitted)	June 2001
972	Sofronis, P., and I. M. Robertson	Atomistic scale experimental observations and micromechanical/ continuum models for the effect of hydrogen on the mechanical behavior of metals—*Philosophical Magazine* (submitted)	June 2001
973	Pushkin, D. O., and H. Aref	Self-similarity theory of stationary coagulation—*Physics of Fluids* **14**, 694–703 (2002)	July 2001
974	Lian, L., and N. R. Sottos	Stress effects in ferroelectric thin films—*Journal of the Mechanics and Physics of Solids* (submitted)	Aug. 2001
975	Fried, E., and R. E. Todres	Prediction of disclinations in nematic elastomers—*Proceedings of the National Academy of Sciences* **98**, 14773–14777 (2001)	Aug. 2001
976	Fried, E., and V. A. Korchagin	Striping of nematic elastomers—*International Journal of Solids and Structures* **39**, 3451–3467 (2002)	Aug. 2001
977	Riahi, D. N.	On nonlinear convection in mushy layers: Part I. Oscillatory modes of convection—*Journal of Fluid Mechanics* **467**, 331–359 (2002)	Sept. 2001
978	Sofronis, P., I. M. Robertson, Y. Liang, D. F. Teter, and N. Aravas	Recent advances in the study of hydrogen embrittlement at the University of Illinois—Invited paper, Hydrogen–Corrosion Deformation Interactions (Sept. 16–21, 2001, Jackson Lake Lodge, Wyo.)	Sept. 2001
979	Fried, E., M. E. Gurtin, and K. Hutter	A void-based description of compaction and segregation in flowing granular materials—*Proceedings of the Royal Society of London A* (submitted)	Sept. 2001
980	Adrian, R. J., S. Balachandar, and Z.-C. Liu	Spanwise growth of vortex structure in wall turbulence—*Korean Society of Mechanical Engineers International Journal* **15**, 1741–1749 (2001)	Sept. 2001
981	Adrian, R. J.	Information and the study of turbulence and complex flow—*Japanese Society of Mechanical Engineers Journal B*, in press (2002)	Oct. 2001
982	Adrian, R. J., and Z.-C. Liu	Observation of vortex packets in direct numerical simulation of fully turbulent channel flow—*Journal of Visualization*, in press (2002)	Oct. 2001
983	Fried, E., and R. E. Todres	Disclinated states in nematic elastomers—*Journal of the Mechanics and Physics of Solids* **50**, 2691–2716 (2002)	Oct. 2001
984	Stewart, D. S.	Towards the miniaturization of explosive technology—Proceedings of the 23rd International Conference on Shock Waves (2001)	Oct. 2001
985	Kasimov, A. R., and Stewart, D. S.	Spinning instability of gaseous detonations—*Journal of Fluid Mechanics* (submitted)	Oct. 2001
986	Brown, E. N., N. R. Sottos, and S. R. White	Fracture testing of a self-healing polymer composite—*Experimental Mechanics* (submitted)	Nov. 2001
987	Phillips, W. R. C.	Langmuir circulations—*Surface Waves* (J. C. R. Hunt and S. Sajjadi, eds.), in press (2002)	Nov. 2001
988	Gioia, G., and F. A. Bombardelli	Scaling and similarity in rough channel flows—*Physical Review Letters* **88**, 014501 (2002)	Nov. 2001
989	Riahi, D. N.	On stationary and oscillatory modes of flow instabilities in a rotating porous layer during alloy solidification—*Journal of Porous Media*, in press (2002)	Nov. 2001
990	Okhuysen, B. S., and D. N. Riahi	Effect of Coriolis force on instabilities of liquid and mushy regions during alloy solidification—*Physics of Fluids* (submitted)	Dec. 2001

List of Recent TAM Reports (cont'd)

No.	*Authors*	*Title*	*Date*
991	Christensen, K. T., and R. J. Adrian	Measurement of instantaneous Eulerian acceleration fields by particle-image accelerometry: Method and accuracy—*Experimental Fluids* (submitted)	Dec. 2001
992	Liu, M., and K. J. Hsia	Interfacial cracks between piezoelectric and elastic materials under in-plane electric loading—*Journal of the Mechanics and Physics of Solids* (submitted)	Dec. 2001
993	Panat, R. P., S. Zhang, and K. J. Hsia	Bond coat surface rumpling in thermal barrier coatings—*Acta Materialia*, in press (2002)	Jan. 2002
994	Aref, H.	A transformation of the point vortex equations—*Physics of Fluids* **14**, 2395–2401 (2002)	Jan. 2002
995	Saif, M. T. A, S. Zhang, A. Haque, and K. J. Hsia	Effect of native Al_2O_3 on the elastic response of nanoscale aluminum films—*Acta Materialia* **50**, 2779–2786 (2002)	Jan. 2002
996	Fried, E., and M. E. Gurtin	A nonequilibrium theory of epitaxial growth that accounts for surface stress and surface diffusion—*Journal of the Mechanics and Physics of Solids*, in press (2002)	Jan. 2002
997	Aref, H.	The development of chaotic advection—*Physics of Fluids* **14**, 1315–1325 (2002); see also *Virtual Journal of Nanoscale Science and Technology*, 11 March 2002	Jan. 2002
998	Christensen, K. T., and R. J. Adrian	The velocity and acceleration signatures of small-scale vortices in turbulent channel flow—*Journal of Turbulence*, in press (2002)	Jan. 2002
999	Riahi, D. N.	Flow instabilities in a horizontal dendrite layer rotating about an inclined axis—*Proceedings of the Royal Society of London A* (submitted)	Feb. 2002
1000	Kessler, M. R., and S. R. White	Cure kinetics of ring-opening metathesis polymerization of dicyclopentadiene—*Journal of Polymer Science A* **40**, 2373–2383 (2002)	Feb. 2002
1001	Dolbow, J. E., E. Fried, and A. Q. Shen	Point defects in nematic gels: The case for hedgehogs—*Proceedings of the National Academy of Sciences* (submitted)	Feb. 2002
1002	Riahi, D. N.	Nonlinear steady convection in rotating mushy layers—*Journal of Fluid Mechanics* (submitted)	Mar. 2002
1003	Carlson, D. E., E. Fried, and S. Sellers	The totality of soft-states in a neo-classical nematic elastomer—*Proceedings of the Royal Society A* (submitted)	Mar. 2002
1004	Fried, E., and R. E. Todres	Normal-stress differences and the detection of disclinations in nematic elastomers—*Journal of Polymer Science B: Polymer Physics*, in **40**, 2098–2106 (2002)	June 2002
1005	Fried, E., and B. C. Roy	Gravity-induced segregation of cohesionless granular mixtures—*Lecture Notes in Mechanics*, in press (2002)	July 2002
1006	Tomkins, C. D., and R. J. Adrian	Spanwise structure and scale growth in turbulent boundary layers—*Journal of Fluid Mechanics* (submitted)	Aug. 2002
1007	Riahi, D. N.	On nonlinear convection in mushy layers: Part 2. Mixed oscillatory and stationary modes of convection—*Journal of Fluid Mechanics* (submitted)	Sept. 2002
1008	Aref, H., P. K. Newton, M. A. Stremler, T. Tokieda, and D. L. Vainchtein	Vortex crystals—*Advances in Applied Mathematics* **39**, in press (2002)	Oct. 2002
1009	Bagchi, P., and S. Balachandar	Effect of turbulence on the drag and lift of a particle—*Physics of Fluids* (submitted)	Oct. 2002
1010	Zhang, S., R. Panat, and K. J. Hsia	Influence of surface morphology on the adhesive strength of aluminum/epoxy interfaces—*Journal of Adhesion Science and Technology* (submitted)	Oct. 2002